JOURNAL OF GEOPHYSICAL RESEARCH, VOL. 107, NO. E12, 5121, doi:10.1029/2001JE001831, 2002

Fate of outflow channel effluents in the northern lowlands of Mars: The Vastitas Borealis Formation as a sublimation residue from frozen ponded bodies of water

Mikhail A. Kreslavsky
Department of Geological Sciences, Brown University, Providence, Rhode Island, USA
Kharkov Astronomical Observatory, Kharkov, Ukraine

James W. Head
Department of Geological Sciences, Brown University, Providence, Rhode Island, USA

Received 5 December 2001; revised 8 April 2002; accepted 20 May 2002; published 7 December 2002.

[1] We analyze the fate of the Hesperian-aged outflow channel effluents emplaced into the northern lowlands of Mars. We have modeled the evolution of these effluents under the assumption that they were emplaced under a range of atmospheric conditions comparable to those of today and thought to have prevailed in the Hesperian. Under these conditions we find that the evolution of the sediment-loaded water after it left the channels includes three phases. Phase 1: Emplacement and intensive cooling: Violent emplacement of water followed by a short period of intensive evaporation from the surface and near-surface layer, and intensive convection. During this phase the water maintained and redistributed its large suspended sediment load. Water vapor strongly influenced the climate, at least for a geologically short time. When the temperature of the water reached the temperature of the maximum density or the freezing point, boiling and intensive convection ceased and the water deposited the sediments. Phase 2: Freezing solid: Geologically rapid freezing of the water body accompanied by weak convective water movement occurred over a period of the order of $\sim 10^4$ years. Phase 3: Sublimation and loss: This period involved sublimation of the ice and lasted longer than the freezing phase. The rate and latitudinal dependence of the sublimation, as well as the location of water vapor condensation, crucially depend on the planetary obliquity, climate, and sedimentary veneering of the ice. Phase 3 would have been very short geologically ($\sim 10^5 - 10^6$ years) if an insulating sedimentary layer did not build up rapidly. If such an insulating layer did form rapidly, sublimation could cease and residual ice hundreds of meters thick could remain below the surface today. The northern lowlands of Mars are largely covered by the Late Hesperian-aged Vastitas Borealis Formation (VBF), which has sharp boundaries clearly seen in the map of kilometer-scale roughness, and a distinctive kilometer-scale roughness signature. We examine detrended topography data and find evidence that the VBF is underlain at very shallow depths by an Early Hesperian ridged volcanic plains substrate, rather than frozen water deposits remaining from the outflow channel events. Analysis of the VBF roughness characteristics suggests at least 100 m thickness of sediments on top of the underlying volcanic ridged plains. The total inferred volume of the VBF material approximately corresponds to the volume of material removed from the outflow channels. These results support a model in which the Vastitas Borealis Formation predominantly represents the sedimentary residue remaining after the sediment-laden water effluents of the outflow channels ponded in the northern lowlands and rapidly froze solid and sublimed. The distinctive facies of the VBF are interpreted to be related to the freezing, sublimation, and residue of the outflow channel effluents. Ridged facies are dominantly marginal and are interpreted to be related to ice sheet lateral retreat. Knobby facies occur throughout and are interpreted to be due to a variety of causes, including dewatering, de-icing and brine-related processes, and kame-like ice residues. Grooved facies are interpreted to represent postsublimation uplift and fracturing

0148-0227/02/2001JE001831$09.00

due to load removal. The mottled facies may represent bright ejecta whose albedo is related to buried sedimentary or evaporitic residues. Presently, the most likely sites to find frozen remnants of the Hesperian ocean are below the floors of stealth craters underlying the VBF. On the basis of these findings and interpretations, we make predictions for the fate of the outflow channel water vapor and the nature of the Martian hydrologic cycle during the Hesperian. If Noachian-aged oceans existed, conditions at that time would be similar to those described for a Hesperian ocean as soon as a global cryosphere was formed. If any residual deposits remain in the northern lowlands from a proposed Noachian ocean, they would lie below both the VBF and the underlying sequence of Hesperian ridged plains. *INDEX TERMS:* 6225 Planetology: Solar System Objects: Mars; 4267 Oceanography: General: Paleoceanography; 5470 Planetology: Solid Surface Planets: Surface materials and properties; 5416 Planetology: Solid Surface Planets: Glaciation; 5407 Planetology: Solid Surface Planets: Atmospheres—evolution; *KEYWORDS:* Mars, oceans, outflow channels, water, sublimation, Vastitas Borealis Formation

Citation: Kreslavsky, M. A., and J. W. Head, Fate of outflow channel effluents in the northern lowlands of Mars: The Vastitas Borealis Formation as a sublimation residue from frozen ponded bodies of water, *J. Geophys. Res.*, *107*(E12), 5121, doi:10.1029/2001JE001831, 2002.

1. Introduction

[2] Discovery of the outflow channels ringing the northern lowlands of Mars (Figure 1) and documentation of their characteristics has led to a long debate about their mode of origin, the nature of the medium involved, their sedimentary load, the duration and synchroneity of flow, and the fate of their effluents (see review by *Carr* [1996a, and references therein]). Most workers favor water as the major outflow-channel forming medium, but considerable uncertainty remains about the role of other volatiles (e.g., CO_2 [*Hoffman*, 2000; *Hoffman et al.*, 2001]), the amount of sediment involved (e.g., sediment-charged floods or water-rich debris flows), and whether or not large standing bodies of water were formed as a result of their emplacement (e.g., the Oceanus Borealis of *Baker et al.* [1991]).

[3] Key to the understanding of the northern lowlands is the nature and origin of the geologic units that represent the sequence of events that occurred there [e.g., *Scott and Tanaka*, 1986; *Tanaka and Scott*, 1987; *Greeley and Guest*, 1987]. One of the most extensive units that occurs in the northern lowlands is the Hesperian-aged Vastitas Borealis Formation (VBF) [*Tanaka and Scott*, 1987], emplaced in a time period comparable to that of the outflow channels (Figure 2). This distinctive unit differs from virtually all others on Mars [*Tanaka and Scott*, 1987], and has surface roughness properties that are unique among Martian geological units, displaying smoothness and a characteristic roughness versus scale dependence [*Kreslavsky and Head*, 1999, 2000]. Recent work on the roughness properties of the Vastitas Borealis Formation and detrended topography of the northern lowlands has suggested that there may be a relation between the formation of the outflow channels and the emplacement of the Vastitas Borealis Formation [e.g., *Head et al.*, 2002].

[4] Some workers have proposed that the northern lowlands were the site of large standing bodies of water [e.g., *Clifford and Parker*, 2001, and references therein] and that the outer contacts of northern lowland units (including the Vastitas Borealis Formation) represent paleoshorelines [e.g., *Parker et al.*, 1989, 1993]. Tests of this hypothesis showed

Figure 1. (opposite) (a) Northern hemisphere topography (MOLA topography superimposed on altimetric gradient map) and locations of major features. The major outflow channels debouch into the northern lowlands in the area surrounding Chryse Planitia (lower left). (b) Map of the kilometer-scale surface roughness of Mars. The map is a composite RGB image. The median absolute values of the differential slopes at 0.6, 2.4, and 9.6 km baselines are used as the blue, green, and red channels, respectively. Brighter shades denote a rougher surface. See *Kreslavsky and Head* [2000] for further details. Outline of the edge of the Vastitas Borealis Formation (light green tone) as inferred from the roughness map is shown in yellow. Note the close correspondence of these boundaries with those mapped geologically from Viking Orbiter images in Figure 1c. (c) Geological map of the northern hemisphere, showing the locations of exposed areas of the Vastitas Borealis Formation and selected areas of deposits that are interpreted to be overlain and underlain by the Vastitas Borealis Formation. Vastitas Borealis Formation (Hv); Hvk (knobby), blue; Hvr (ridged) olive; Hvm (mottled) light blue gray; Hvg (grooved), yellow green. Areas of underlying Hr (ridged plains) are shown in red. Older, heavily cratered terrain is seen in the surrounding uplands (topographically pitted by craters), and smoother volcanic units of Tharsis and Elysium are largely Amazonian in age. A tongue-like lobe of Amazonian-aged Elysium flow deposits, Ael_3 (green), extends into the Utopia basin and overlies the Vastitas Borealis Formation. Amazonian-aged polar (white) and circumpolar mantled units, Am (orange), overlie the Vastitas Borealis in the center. Amazonian-aged deposits marginal to the northern lowlands (not shown) include smooth plains and members of the Arcadia Formation. Note numerous outflow channels debouching into the Chryse Basin (lower left). A thin Late Amazonian latitude-dependent mantle (not shown) covers the Vastitas Borealis Formation northward from ~47° latitude; see [*Kreslavsky and Head*, 2000]. Compiled from *Tanaka and Scott* [1987], *Scott and Tanaka* [1986], and *Greeley and Guest* [1987], to which reference can be made for detailed unit designations. Superposed on MOLA altimetric gradient map. See a) for locations, major features, and topographic details.

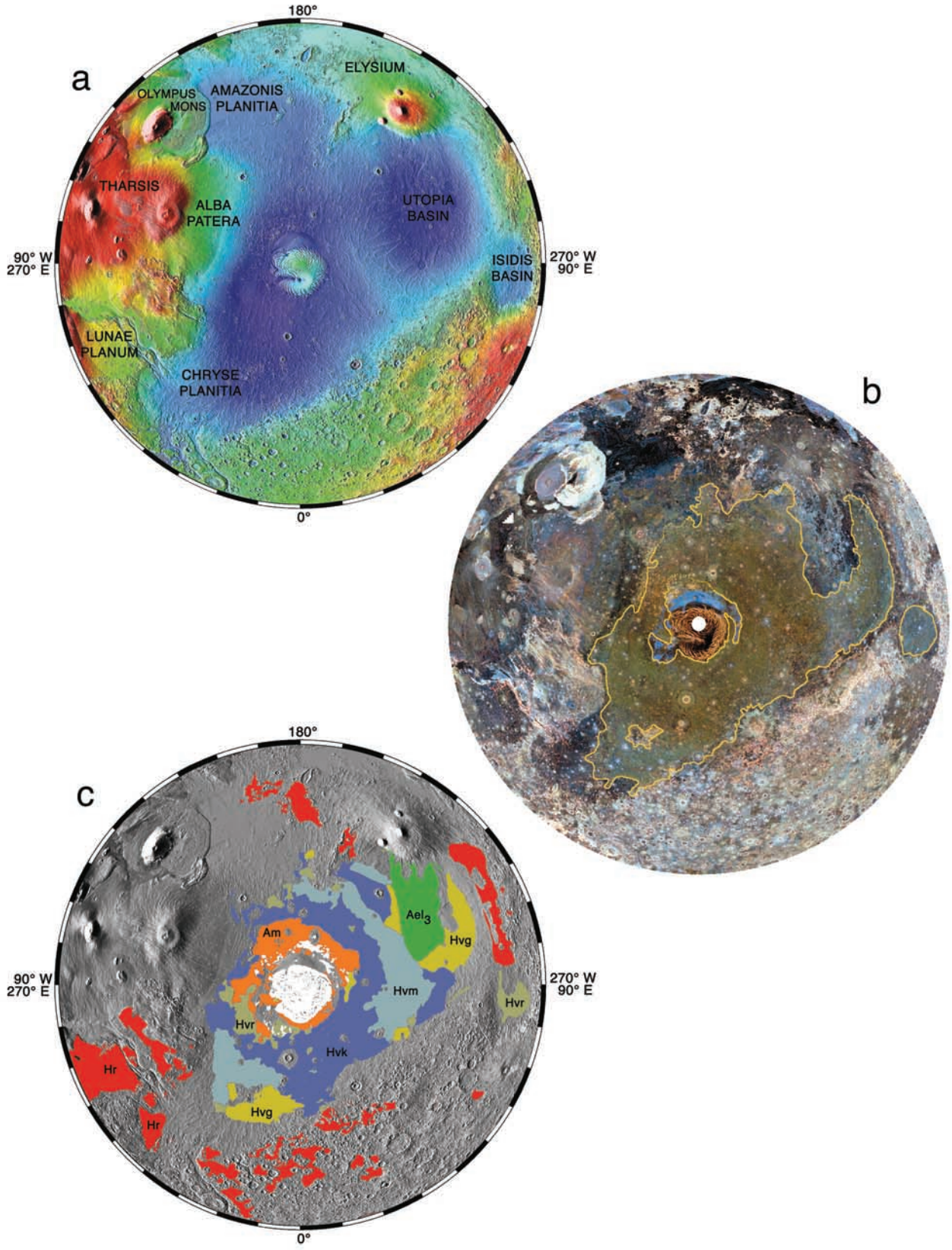
a
180°
ELYSIUM
OLYMPUS MONS
AMAZONIS PLANITIA
THARSIS
ALBA PATERA
UTOPIA BASIN
90° W 270° E
270° W 90° E
ISIDIS BASIN
LUNAE PLANUM
CHRYSE PLANITIA
0°
b
c
180°
Am
Ael3
Hvg
Hvm
Hvr
Hvr
Hvk
Hr
Hvg
Hr
90° W 270° E
270° W 90° E
0°

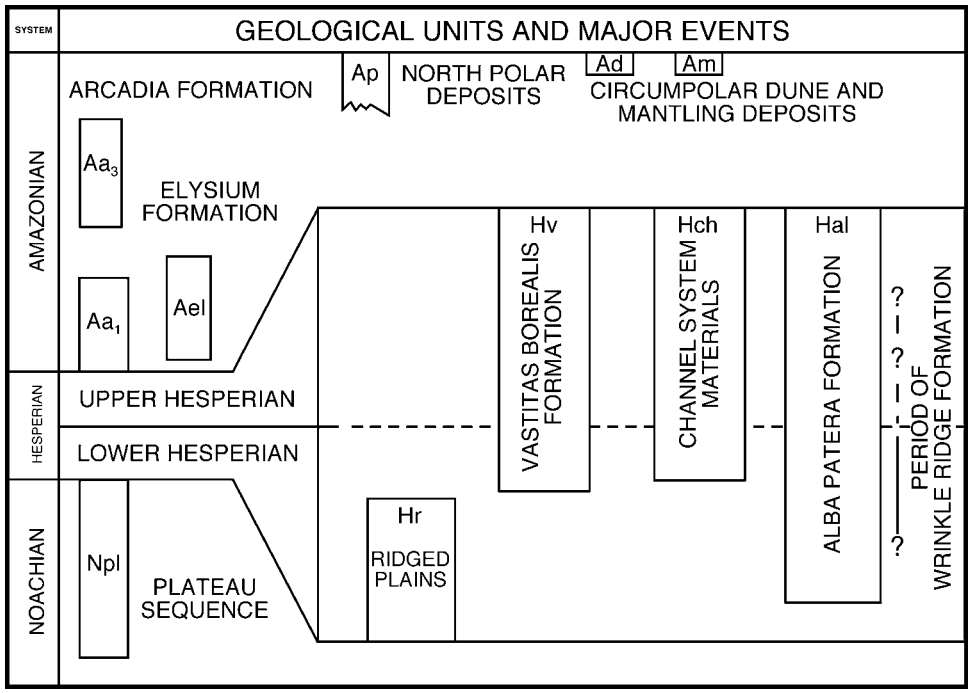

Figure 2. Correlation of map units and geologic events in the Hesperian. The stratigraphy and geological history of the northern lowlands of Mars is modified from 1:15,000,000 USGS geological maps of Mars [*Scott and Tanaka*, 1986; *Tanaka and Scott*, 1987; *Greeley and Guest*, 1987]. The ridged plains (Hr) is Early Hesperian in age and underlies the later Vastitas Borealis Formation (Hv) and outflow channel system materials (Hch), which are contemporaneous and Late Hesperian in age. Noachian unit Npl is the plateau sequence and includes several subunits [Npl_1 (cratered unit), Npl_2 (subdued cratered unit), Npld (dissected unit), and Nplr (ridged unit)]. Hesperian unit Hch is channel system materials and consists of two subunits [Hch (channel material) and Hchp (channel floodplain material)]. The Arcadia Formation consists of several members, two of which are shown here. Aps, smooth plains of Amazonian age, and HNu, an undivided unit forming hills and mesas several to more than 10 km across, are not shown in this figure. Activity at Alba Patera persisted throughout much of the Hesperian (Hal). The interpreted period of formation of wrinkle ridges superposed on Hr, and the laterally equivalent unit underlying the Vastitas Borealis Formation in the northern lowlands [*Head et al.*, 2002] is shown by the vertical line.

that the older of the two contacts was not representative of an equipotential line that might be consistent with a shoreline interpretation, but that the younger contact (corresponding generally to the outer edge of the Vastitas Borealis Formation) represented a much closer approximation, although with some major variations [e.g., *Head et al.*, 1999].

[5] In this paper we pursue the testing of hypotheses for the emplacement of outflow channel effluent and its fate. In order to begin to test the full range of hypotheses, we first pursue an end-member hypothesis for outflow channel formation and effluent ponding and evolution. We assume: 1) that outflow channel formation emplaced significant quantities of water and sediment into the northern lowlands over a geologically short period of time largely in the Late Hesperian [e.g., *Scott and Tanaka*, 1986; *Greeley and Guest*, 1987], and 2) that the atmospheric conditions were near to those that exist on Mars today [e.g., *Melosh and Vickery*, 1989]. We are aware that CO_2-related processes can play a role in shaping the surface of Mars [e.g., *Hoffman*, 2000], however, we do not address this in the present work. We then examine variations on these assumptions and compare the results to the observed geological record. Finally, we examine the hypothesis that the temporally correlative Vastitas Borealis Formation (Figure 2) represents the sublimation residue from frozen ponded bodies of water resulting from the emplacement and evolution of outflow channel effluents.

2. Fate of Water Emplaced on the Surface of Mars

2.1. Phase 1: Outflow Events and Warm Ocean

2.1.1. Outflow Events

[6] The fate of water catastrophically discharged from the outflow channels depends to some extent on the water temperature and amount of dissolved salts. This, in turn, depends on the particular mechanisms of the high-discharge-rate outflows responsible for the formation of the outflow channels, which are not clear in detail [*Carr*, 1996a].

[7] A number of authors have considered release of liquid water from a subsurface aquifer [e.g., *Clifford*, 1993; *Clifford and Parker*, 2001, and references therein]. The morphologically inferred high discharge rates demand a rather short duration for the event (days to months [e.g., *Carr*, 1996a]). This precludes supply of the water from

distant parts of the planet, even if a global subsurface aquifer exists and the megaregolith has high permeability, as argued by *Clifford* [1993]. Discharged water should be derived locally, for example, within the areas of chaotic terrain associated with the outflow channel source regions [*Carr*, 1996a]. The amount of water released during a single event is on the order of an equivalent of a several meters thick layer over the whole planet. This means that given reasonable porosity of the source region, the water should be derived from depths starting from the melting isotherm (cryosphere base) down to hundreds of meters or even kilometers. The water temperature in the aquifer is controlled by the geothermal gradient. This means that the majority of the discharged water would have temperatures several degrees to tens of degrees above the freezing point. The enhanced geothermal gradient hypothesized for the Tharsis region during the epoch of the major outflow events [e.g., *Baker*, 2001] would increase the temperature.

[8] A basically different mechanism of the outflow events and chaotic terrain formation involves run-away decomposition of CO_2 clathrate hydrate as a source of liquid water [e.g., *Milton*, 1974; *Hoffman*, 2000; *Komatsu et al.*, 2000]. At high pressure, clathrate decomposition starts at 283 K, 10 degrees above the freezing point of pure water. However, clathrate decomposition is an endothermic process, and at lower pressure it goes at lower temperature, which would lead to colder released water. This means that the water formed due to clathrate decomposition can have temperature from 273 K to 283 K. We will consider the consequences of both "cold" (just above the freezing point) and "warm" (several degrees or to tens of degrees warmer) water emplacement.

[9] *Clifford* [1993] and *Clifford and Parker* [2001] argue that the water, after its long life in the global subsurface aquifer, would have a high concentration of dissolved salts. The water formed due to clathrate decomposition would have little salts dissolved. The freezing point of water, T_0, depends on the salt concentration and can vary from 273 K for pure water to 240 K and even lower [e.g., *Brass*, 1980]. Below we will keep in mind the whole range of possible salt content from pure water to concentrated brine.

2.1.2. Warm Ocean

[10] First, we consider the consequences of rapid emplacement of "warm" water. Flow of warm water into the northern lowlands would result in ponding and production of a warm ocean phase, in which water temperature was above the freezing temperature. During this warm ocean phase, the dominant part of water heat would be lost through formation of water vapor (Figure 3). The rapid heat loss from the near-surface water layer would cause intensive convection, which would prevent formation of an ice sheet on the water surface. Some disintegrated ice can be formed, and accumulation of some amount of slush near the surface is possible, however the intensive convection would probably preclude solidification of the slush; thus, formation of the thin slush layer would not reduce the intensive evaporation. If the water is warm enough and atmospheric pressure is low enough, real boiling could occur in the uppermost layers of the water in the locations of convective upwellings (Figure 3).

[11] To lower the temperature of the body of water by 10 degrees, 1.5% of its column-integrated mass should be evaporated, as follows from the ratio of evaporation heat ($L_v \sim 2.8 \times 10^6$ J kg^{-1}) and water specific heat capacity ($c_w \sim 4.2 \times 10^3$ J kg^{-1} K^{-1}). Even a modest outflow event inevitably releases an amount of vapor which is huge in comparison to the present thin Martian atmosphere, or atmospheres thought to have been characteristic of this time [e.g., *Melosh and Vickery*, 1989]. If the northern lowlands were filled approximately to the level of the outer VBF boundary, and the water emerged at the surface having an average temperature of +10°C, the vapor release would correspond approximately to a 1 m deep water layer over the whole planet. Of course, the Martian atmosphere was unable to retain even a small portion of this amount of water. The vast majority of the vapor was immediately condensed. A large part of it fell back to the ocean as snow and was entrained by the convective flow and melted. A part of the water vapor condensed at the solid cold surfaces near the ocean shorelines and probably over the whole planet [e.g., *Head and Kreslavsky*, 2001a, 2001b]. The water vapor release inevitably had a strong impact on climate, at least for a short time. The water vapor atmosphere during the warm ocean phase is very far from equilibrium and is difficult to model [e.g., *Gulick et al.*, 1997].

[12] The evaporation rate can be estimated through the following considerations (similar to those used by *Kargel et al.* [1995]). The heat removed from the floodwater by evaporation is eventually released and radiated to space, when the vapor condenses in the atmosphere or at the surface. The blackbody radiation at the temperature of T_0, $Q_b \sim 300$ W m^{-2} gives a scale for the heat loss rate. The actual water heat loss rate could be lower, because (1) the vapor and clouds do not radiate as a blackbody; (2) some energy is radiated by vapor and clouds at temperature lower than T_0, and (3) some radiated energy covers the heat absorbed from the solar irradiation. On the other hand, several factors could increase the rate: (1) the vapor and clouds can be distributed by winds and radiate from an area larger than the area of the ocean; (2) under some conditions, the warm water surface could radiate immediately to space. We believe that the actual heat loss is within the range of 100–300 W m^{-2}. This is somewhat below the lower boundary of the everyday life concept of boiling. This heat loss rate corresponds to evaporation of 3–9 mm per day or to the same amount of precipitation (if all the vapor goes back locally), which is similar to our everyday life concept of a weak snowfall. Of course, the presence of a highly non-equilibrium transient water vapor atmosphere above the warm ocean could produce much more severe weather conditions locally.

[13] The estimated heat loss rate gives a cooling rate of 7–20 K per year for a 100 m deep body of water. The cooling rate is inversely proportional to the water layer thickness. Regional variations in ocean cooling rates are primarily due to depth variations. They would lead to regional temperature variations in the ocean, which would produce a developed system of currents.

[14] The warm ocean phase would last until the whole body of water cooled down to the freezing point, or, if the salinity is low, to the temperature of the maximum density (~277 K for pure water). After that occurred, the intensive convection would cease, a continuous ice layer would form on the surface and intensive evaporation would stop. The

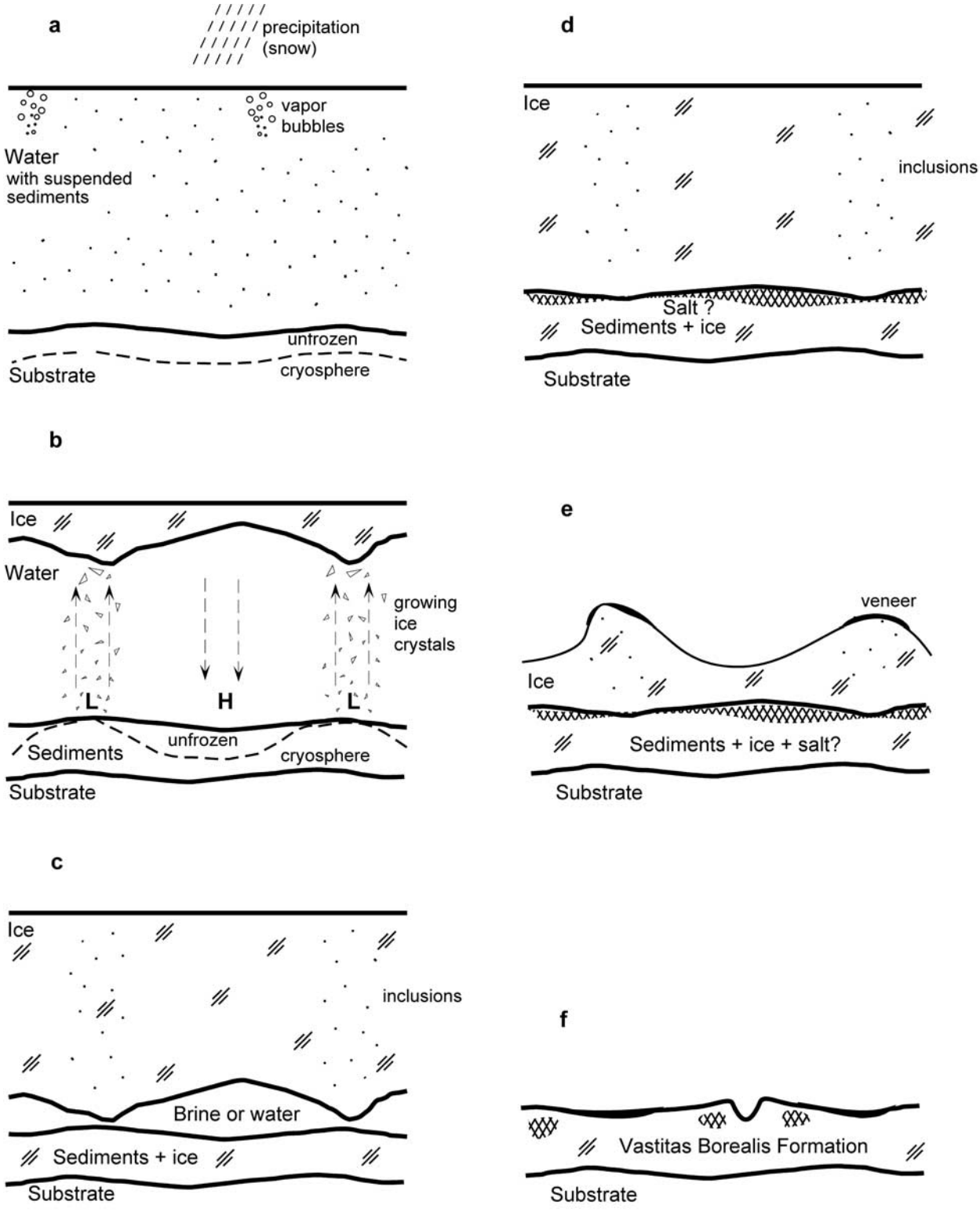

Figure 3. Conceptual diagram illustrating possible steps in the fate of water emplaced and ponded in the northern lowlands of Mars. (a) Warm ocean with intensive turbulent movement keeps sediments suspended, intensive evaporation (some true boiling) leads to intensive precipitation. (b) Freezing ocean with a system of cyclonic eddies (L) and stable anticyclonic eddies (H); sediments are deposited on the basin floor. (c) Almost frozen ocean with pockets of water or brine in the locations of the stable anticyclonic eddies. (d) Frozen ocean with clear ice in the place of the stable anticyclonic eddies, minor amount of sediment inclusions in the areas of cyclonic eddies, and possible salt lenses in the locations of brine pockets. (e) Subliming ice with protective sediment veneer in the areas with sediment inclusions. (f) Residual ice-rich sediments produce the Vastitas Borealis Formation, which is further reworked by impacts and periglacial processes.

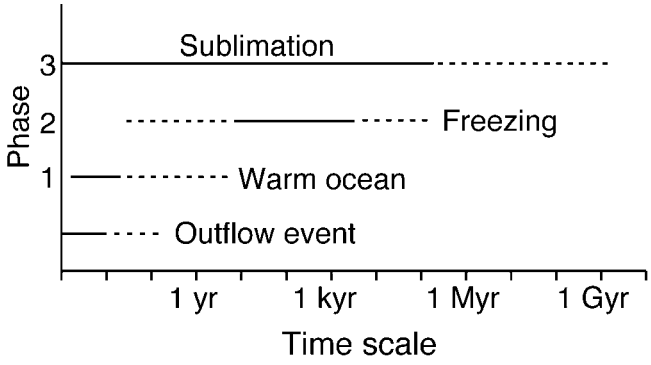

Figure 4. Timescales of sequence of events in the emplacement and sublimation of outflow channel effluents. Following the outflow event, there is a very short warm ocean phase (Phase 1), followed by rapid freezing (Phase 2) and a sublimation phase (Phase 3) that is likely to be geologically short.

duration of the warm ocean phase is approximately proportional to the total amount of heat brought by the outflow event. For an ocean with an initial temperature of 10 K above the freezing or maximum density point, the warm ocean phase would be very short geologically, lasting 3–8 years (Figure 4).

[15] Figure 5 shows schematically the evolution of pressure and temperature at the ocean floor. The emplacement of water during the outflow event will cause rapid build-up of hydrostatic pressure at the floor (segment 1 in Figure 5). Pressure decrease due to evaporation of a part of the water during the phase of warm ocean (segment 2) is negligible, while the temperature decreases to the freezing point. The surface pressure and temperature on the non-flooded parts of Mars are supposed to lie within or close to the shaded area in the diagram (Figure 5), which represents reasonable variations due to obliquity changes. The outflow event and the warm ocean would result in a short-term excursion of the surface conditions like that represented by the question marks in Figure 5.

[16] The outflow events transported a sediment load from the outflow channels into the northern lowlands [e.g., *Carr*, 1996a]. Highly turbulent water flow in the outflow channels was able to maintain a large load of suspended sediments [e.g., *Carr*, 1996a]. Water velocity and the turbulence intensity would decrease significantly when the water reaches the lowlands, and a part of the sediment load would be dropped. The water in the warm ocean, however, would still be moving and turbulent due to intensive convection and systems of currents, and it could still maintain a large sedimentary load, especially its finest size fraction. The suspended sediments could be redistributed over the whole lake or ocean. Local depressions, first of all, the impact craters, served as effective traps for the sediments and were rapidly filled during the initial emplacement event and due to subsequent circulation. When the water reached the temperature of maximal density, the intensity of convection decreased, and the water deposited the major part of its suspended sediment load. The thickness of the resulting suspended sediment layer might be relatively even over the flooded basin but its thickness could vary due to any oceanic circulation pattern, and the presence of local sediment traps, i.e., craters. For example, extreme sedimentation rates of 50 cm per year are known in terrestrial submarine craters [*Thatje et al.*, 1999].

[17] This short and intensive heat loss from the warm ocean (Figures 3–5) will inevitably occur if the initial atmospheric pressure was more or less similar to the

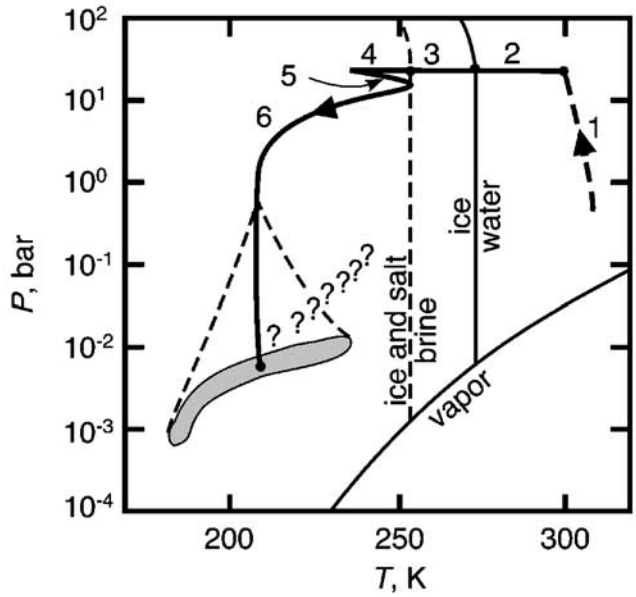

Figure 5. Schematic evolution of pressure (P) and temperature (T) below the water at the floor of the transient ocean (bold lines) superposed over a phase diagram of water (thin solid lines) and schematically-shown salt-water mixture melting point (thin dashed line). Shaded area schematically shows the range of conditions at the surface on Mars throughout obliquity cycles; dot within this range marks the average conditions today. A chain of question marks schematically shows the possible excursion of the conditions at the surface during the geologically short time after the outflow event. Stages of evolution of the transient ocean: 1. Outflow event; hydrostatic pressure builds up below the water; 2. Warm ocean (Phase 1); temperature at the base of the ocean decreases to the water melting point. 3. Freezing ocean (Phase 2); salt concentration increases at the base of the ocean, temperature decreases to the point of brine solidification. 4. Further cooling of ice at the base. 5. Steady state thermal gradient is established; some heating occurs due to the geothermal flux; brine mobilization [*Head and Pappalardo*, 1999] might be possible; minor decrease of pressure is due to sublimation at the surface. 6. Sublimation (Phase 3); temperature drops approximately along the ice geotherm. Behavior from this point to preexisting surface conditions is unknown because of the range of possible surface conditions (shaded area) during obliquity cycles. The solid line extends to present conditions, the dashed lines define the envelope of possibilities. Note that surface conditions on the non-flooded parts of Mars during this geologically short period of time (see Figure 4) are very likely to lie within the shaded range, with possible short-term excursions like that represented by the question marks.

present. *Baker et al.* [1991] hypothesized that major outflow events could be accompanied by the release of huge amounts of CO_2 to the atmosphere (up to 4 bars surface pressure). If this happened, the evaporation would be slower, although a generally similar set of processes would occur in the warm ocean. Water cooling would be slower, convection would be less intensive, and a larger proportion of sediments would be dropped near the outflow channel mouths. Release of large amounts of CO_2 would have a strong and long lasting effect on the mean surface temperature and on the climate in general [*Gulick et al.*, 1997].

2.1.3. Cold Floods

[18] If the floodwater was "cold", that is the temperature was very close to the freezing point for salty water or below the maximal density point for fresh water, the "warm ocean" phase would be skipped, and the ice lid would start forming immediately after the water came to the lowlands. The main difference from the case of "warm" water outflow is that there would be no intensive convection and circulation. The intensive turbulence of flowing water would cease quickly just after the water leaves the channel and reaches the lowlands, and the major part of the suspended sediment load would be deposited immediately close to the channel mouth.

2.2. Phase 2: Freezing Ocean

[19] After the ice sheet on the surface of the lake or ocean started to form, the intensive evaporation would be suppressed, the heat release would get much slower (Figures 3 and 4), and the immediate influence of the ocean on the climate would become weaker. The ice layer on the surface of the ocean would grow, until the whole ocean would freeze solid. The value of the geothermal heat flux necessary to prevent the deepest parts of the ocean from freezing [e.g., *Clifford and Parker*, 2001] is unreasonably high for the Later Hesperian. The water temperature in the freezing ocean would be very close to the freezing point, which would gradually decrease due to increase of salinity of the residual liquid.

2.2.1. Freezing Time

[20] To freeze, the water needs to give out the latent heat of fusion. This heat can be transferred to the surface through the growing ice sheet at the upper water surface, and also transferred to the floor, which had been cold before the water emplacement. The rate of these two processes defines the rate of freezing. As we well show later, the sublimation rate of the ice is lower than the freezing rate. The heat loss through the upper ice sheet was quantitatively assessed by a number of authors [e.g., *Carr*, 1983; *Moore et al.*, 1995; *Kargel et al.*, 1995]. The heat loss to the substrate was generally ignored. Below we consider characteristic rate and timescale of freezing controlled by these two processes.

[21] If we ignore for the moment the heat transfer to the substrate, the heat loss through the growing ice sheet would lead to an increase of the ice thickness h with time t according to the classic approximate formula [e.g., *Hobbs*, 1974]

$$h(t)\sqrt{\frac{2\kappa_i(T_0 - T_s)}{L_i\rho_i}}\sqrt{t}, \tag{1}$$

where T_s is the year-average surface temperature, T_0 is the water freezing point (depends on salinity), ρ_i is the density of ice, $\kappa_i = 2.5$ W m^{-1} K^{-1} is the thermal conductivity of ice, $L_i = 3.3 \times 10^5$ J kg^{-1} is the fusion heat of ice. This equation approximates the rigorous result used by *Moore et al.* [1995] with high accuracy. The formation of the ice sheet of thickness h takes time

$$t(h) = \frac{L_i\rho_i}{2\kappa_i(T_0 - T_s)}h^2. \tag{2}$$

If we suggest $T_0 - T_s \sim 60$ K to represent fresh water and typical present surface conditions, equation (2) gives $t(h) \sim$ 33,000 yr km$^{-2}h^2$, that is, for example, 33,000 years for 2 km deep ocean, or ~9,000 years for 0.5 km deep ocean. These estimates agree with similar estimates from the references mentioned above.

[22] Let us now ignore for the moment the heat loss through the ice sheet and consider the heat transfer to the substrate. If we suppose that the substrate had the year-average surface temperature T_s before the water emplacement, and the geothermal gradient of G, the growth of the ice sheet with time due to heat transfer to the substrate would be described as

$$h(t)1.6\frac{\sqrt{\kappa_s c_s \rho_s}}{L_i\rho_i}(T_0 - T_s)\sqrt{t} - \frac{\kappa_s G}{L_i\rho_i}t, \tag{3}$$

where κ_s, c_s, and ρ_s are the thermal conductivity, specific heat and density of the substrate, and G is the geothermal gradient in the substrate. For the early stages of freezing the second term in (3) is negligible, and the rates of ice growth predicted by (1) and (3) are proportional to each other. Their ratio is

$$1.1\left(\frac{\kappa_s}{\kappa_i}\frac{\rho_s}{\rho_i}\frac{c_s(T_0 - T_s)}{L_i}\right)^{1/2}. \tag{4}$$

For a typical value of thermal conductivity of rocks $\kappa_s = 1.5$ W m^{-1} K^{-1} and $T_0 - T_s \sim 60$ K this ratio is ~0.7. The thermal conductivity of the substrate is not known accurately (see, e.g., discussion by *Clifford* [1993]); however, all reasonable variations together with variations of the surface temperature and salinity will result this ratio falling within a range of 0.5–1. Thus the heat transfer to the substrate makes a contribution to the freezing rate comparable to the freezing rate due to heat loss through the growing ice sheet, though somewhat lower.

[23] When both processes work together, the ice added due to the cryosphere heating reduces the rate of conductive cooling through the ice sheet. The resulting ice growth rate will be lower than the sum of the rates due to both mechanisms, but still higher than the rate predicted by (1). Thus, we conclude that the total time of freezing is several tens of percent shorter than predicted by equation (2). Taking into account all uncertainties in parameters (supposing, however, that the climate is more or less similar to the present), we conclude that the freezing time is within the range of 8,000 to 30,000 yr km$^{-2}h^2$, where h is the initial water depth (or final ice thickness). For example, for a 0.5-km deep ocean this gives 2,000–7,500 years.

2.2.2. Transient Thinning of the Cryosphere

[24] As we saw above, a noticable part of heat brought to the lowlands with the water would go to the substrate and

heat it up. The upper part of the substrate is the so-called cryosphere [e.g., *Clifford*, 1993], the layer, where the temperature is below the water freezing point. Its thickness is $H_c \sim (T_0 - T_s)/G$. Heating the substrate moves the melting isotherm in the substrate upward. If the melting isotherm reached the floor of the ocean, the cryosphere would disappear, which might have important hydrological implications [e.g., *Clifford*, 1993; *Clifford and Parker*, 2001]. If we ignore for the moment the heat transfer through the growing ice sheet, the thickness of the freezing water layer necessary to bring the melting isotherm in the substrate to the floor is

$$h_c = 0.64 \frac{\rho_s}{\rho_i} \frac{c_s}{L_i} (T_0 - T_S) H_c \sim \frac{T_0 - T_s}{120\ \mathrm{K}} H_c. \quad (5)$$

If we take into account the heat transfer through the growing ice sheet, the thickness of water necessary to destroy the cryosphere would be at least 2 times greater than predicted by (5), and even greater, because when the melting isotherm approaches the surface, the rate of heat transfer to the substrate decreases (the second term in (3) becomes non-negligible). For the present conditions this means that $h_c > H_c$, that is the destruction of the cryosphere, demands an amount of water greater than the initial cryosphere thickness. For high latitudes (higher $T_0 - T_s$) even more water is necessary. The global ocean in the northern lowlands would have a maximal depth of about 1.5 km at rather high latitude, and less than a kilometer in its low-latitude parts. This means that the transient destruction of the cryosphere due to the emplacement of water is only possible if the cryosphere was thinner than 1 km. On the basis of indirect estimates of the geothermal flux in the Hesperian [*Zuber et al.*, 2000], the cryosphere would not have been thin enough to be disrupted (see additional discussion of probable cryosphere thickness by *Clifford and Parker* [2001]).

2.2.3. Currents in a Freezing Ocean

[25] When a fresh-water lake freezes on the Earth, a major volume of water below a certain depth remains at the temperature of the maximum density (~281 K). This depth increases gradually with the heat loss through the ice sheet and the increase of the ice thickness. No convective motion of the water occurs. The situation in the freezing ocean on Mars is different because of cooling from below due to heat transfer to the cryosphere. The water cools at the floor, becomes less dense, and produces a convective current. This convection leads to a reduction of temperature contrasts, and all the water below the growing ice sheet would become very close to the freezing point rather quickly.

[26] If the water bears a sufficient amount of dissolved salts (>2.5% for Earth seawater composition), there is no inverse dependence of the water density on the temperature. In this case the warm ocean phase convection continues until the whole body of water reaches a temperature very close to the freezing point (Figures 3–5).

[27] As soon as all the water is very close to the freezing point, the heat loss to the cryosphere would lead to freezing at the floor. The ice, being buoyant, could leave the floor and move upward. This movement would entrain some surrounding water. The decrease of pressure along this upwelling would lead to increase of the melting point with the rate of $\Gamma_i \approx 0.2$ K km^{-1}. Adiabatic heating due to the pressure decrease is an order of magnitude smaller even for pure water, and is modified with adiabatic cooling for high salinity. The increase of the freezing point would lead to formation of an additional amount of ice in the upwelling water current (~0.25% per km). This would lead to an increase of buoyancy and favor further upwelling. When the upwelling flow reaches the lower surface of the ice sheet, the ice particles would contribute to the growth of the sheet. The water would be liberated from the buoyant load and form a downwelling current. Being close to the cooling ice surface, the water would give some heat to the ice sheet and some additional portion would freeze. This would increase salinity, produce some negative buoyancy, and contribute to the downwelling current.

[28] This simple picture of a specific convective flow will be complicated by the Coriolis force due to planet rotation. Establishing of upwelling and downwelling currents would be accompanied by formation of eddies similar to cyclones and anticyclones, with horizontal velocities of several orders of magnitude greater than vertical currents (Figure 3).

[29] An anticyclonic eddy, once formed, will remain stable over a long time for the following reasons. At the ocean floor, the downwelling current would bring water slightly warmer than the local freezing point, the floor temperature would become above the freezing point, and ice formation would not occur in these areas, which would prevent initiation of upwelling. Outside the anticyclonic eddy, the upwelling would supply additional ice to the ice-water interface. This would make the ice sheet thicker outside the eddy. The thinner ice sheet within the anticyclonic eddy would favor heat transfer to the cold upper surface, which would favor downwelling due to salinity increase. Finally, a closed area of thicker water layer would dynamically favor a stability of rotating water motion (e.g., a "Taylor column") [e.g., *Cushman-Roisin*, 1994]. This long-term stability of the anticyclonic eddies would lead, after a period of rather chaotic motion of cyclonic eddies, to formation of a network of stable anticyclonic eddies of more or less similar size. Smaller cyclonic eddies would migrate between larger anticyclonic eddies.

[30] The formation of an eddy network would lead to a cell-like topography of the ice-water interface, with rounded thinner areas at the locations of the anticyclonic eddies. When most of the water freezes, the ice would first reach the floor in the former upwelling areas and leave the cells of water in the places of former anticyclonic eddies. If the water initially contained dissolved salts, all the salt will remain in these unfrozen cells. After complete freezing the exsolved salts would produce a specific topography of the ocean floor, with rounded heights at the places of the former anticyclonic eddies. A typical Earth seawater salinity corresponds to a salt layer of approximately 1.5% of the seawater layer. This provides a rough estimate of the possible amplitude of the floor topography produced with this mechanism. For example, for a 0.6 km deep ocean, the salt layer topography can vary within ~8 m.

[31] As the ice sheet forms, the salinity of the remaining water will increase. The rate of this increase would be higher in the initially shallower areas of the ocean. This would lead to salinity gradients approximately correspond-

ing to topographic gradients of the seafloor. These regional salinity gradients would lead to formation of a system of regional currents. Due to the Coriolis force the current lines would approximately follow the floor topography contours.

2.2.4. Tides in the Freezing Ocean

[32] For a planet covered with a deep inviscid ocean, the maximal tide amplitude is scaled as:

$$h = \frac{GMR^2}{gr^3}, \quad (6)$$

where R is the planet's radius, g is the acceleration due to gravity at its surface, M is the mass of the body causing tides, r is the distance from this body to the planet, and G is the gravity constant. This gives 3.4 cm for solar tides on Mars (compared to 37 cm for lunar tides on the Earth). Tides due to Phobos are an order of magnitude smaller; tides due to Deimos are negligible in comparison to tides due to Phobos. The presence of some freely floating ice does not influence the tide amplitude. The tide amplitude given by (6) is effective for an equatorial zone of the planet. For high latitudes it is reduced by a factor of $\sim\cos^2(\lambda)$, where λ is the latitude. This factor also weakly depends on the season. If the ocean is not global, the tide amplitude is reduced by a factor of $\sim(l/R)^2$ where l is the linear size of the ocean. This means that for small isolated seas and lakes tides are negligible. All these considerations show that the tidal amplitude in an open ocean on Mars is $\sim$1 cm or smaller, and tides in an open ocean are very unlikely to produce observable morphological features.

[33] On the Earth the tidal amplitude in many ocean shores exceeds the tidal amplitude in the open ocean by an order of magnitude and more. This occurs due to resonances. In some sites, the tides enhanced by resonances could have an amplitude of up to a meter. An ice sheet moved by tides can act as an effective eroding agent, producing observable morphological features at some locations (see discussion by *Thomson and Head* [2001]).

2.3. Phase 3: Frozen Ocean

2.3.1. Sublimation Rates

[34] After the water froze, the most prominent process was the sublimation of ice (Figures 3–5). The sublimation rate is poorly constrained in comparison to the freezing rate, and the dynamics of a candidate frozen ocean should be derived from geological observations and compared to simple physical considerations. For example, even for the present observed polar caps, the sublimation rate is not known, and estimations are rather uncertain (see discussion by *Ivanov and Muhleman* [2000]). The sublimation rate for a bare ice or snow surface is sensitive to solar irradiation, atmospheric pressure, winds, and surface structure. *Jakosky and Haberle* [1992] gave an estimate of the sublimation rate of 0.1–0.8 mm per season for the present polar cap. The rate of 0.8 mm per season leads to sublimation of a 0.5 km thick layer of ice in 1.5 Myr. For lower latitudes or higher obliquity the sublimation rate can be higher. Estimates by *Toon et al.* [1980] gave rates as high as 0.5 m per year for the pole at favorable conditions (high obliquity, strong winds). These high sublimation rates give a timescale for sublimation (a thousand years) comparable to the timescale of freezing previously described (Figure 4). *Moore et al.* [1995] obtained a sublimation time for a 1-km-thick ice layer at current obliquity and low latitude (25°) as within 0.1–1.6 Myr.

[35] The sublimation rate would be strongly influenced by coverage of the ice with a sheet of sediments. Such a sheet could result from sublimation, if the ice contained some admixture of solid particles. The uppermost thin layer of ice formed at the end of the warm ocean phase would contain a certain amount of inclusions from the suspended sediment load. Sublimation of this layer could give up to several mm of soil on the surface. As we saw above (section 2.2.3), freezing at the ocean floor could bring up to meters (probably less) of sediments into the base of the ice sheet. In the course of sublimation these sediment particles could accumulate at the surface. Another source for the sediment veneer can be deposition of wind-blown material. On the other hand, wind action should also remove the veneer and favor sublimation. A globally averaged sedimentation rate of $\sim$7 microns per year was inferred by *Pollack et al.* [1979] from Viking observations of atmospheric dust loading during the global dust storm. Assuming a global dust storm to occur every $\sim$10 years, this suggests a characteristic thickness of a dust layer of $\sim$1 m that would be deposited or removed in 1 Myr. Of course, this number could vary within several orders of magnitude both regionally and temporally. Observations at the surface of the northern lowlands by Viking 1 [*Binder et al.*, 1977], Viking 2 [*Mutch et al.*, 1977], and Pathfinder [*Greeley et al.*, 1999] show evidence for both erosion and deposition of fine fragmental material, suggesting an active layer over the timescales considered here. Layers of impact ejecta or widely dispersed volcanic tephra [*Wilson and Head*, 1994] could also form sediment layers on top of the ice.

[36] The presence or absence of a sediment veneer can change the sublimation rate by many orders of magnitude. A hundred meter thick layer of sediment covering the ice could effectively prevent sublimation, as follows from the estimations of ground ice stability [e.g., *Squyres et al.*, 1992; *Mellon and Jakosky*, 1993, 1995]. Estimations by *Carr* [1990] showed that even for a one-meter-thick veneer, the sublimation rate is reduced to 10 cm per 1 Myr and lower, which gives a lifetime for the frozen ocean of about the age of the planet or longer. Estimates of the vapor diffusion rates in porous media, however, crucially depend on pore sizes, and the rates for a layer of the same thickness can vary several orders of magnitude (see also discussion by *Clifford and Parker* [2001]). Thus, the actual rates of sublimation cannot be inferred from a priori considerations, and we need to look for geological evidence for the lifetime of the ice sheet.

[37] The spatial pattern of the ice sublimation rate is controlled by the presence and thickness of the veneer. However, it is interesting to consider the latitudinal pattern of the sublimation rate, if we assume a uniform veneer. If the veneer is absent or very thin ($<\sim$1 cm), the sublimation rate is controlled by the maximum surface temperature, actually, by the summer noon sun height. In this case for a moderate obliquity ($<\sim$35°) the sublimation rate at the southern margins of the northern lowlands would be much faster than in the vicinity of the pole. If the veneer is several tens of centimeters thick, the sublimation rate is defined by the maximal (summer) day-average temperature of the sur-

face, actually, by the day-average solar irradiation at the solstice. The latitudinal variations of this parameter are minor for moderate obliquity (15°–30°); for lower obliquity the pole is colder, for higher obliquity it is warmer. Finally, for a thicker veneer (>∼1 m), the year-average surface temperature becomes important. Here again the latitudinal dependence for low and moderate obliquity (<∼30°) is strong. The year-average solar irradiation of the pole reaches that for the equator for an obliquity of 54°.

[38] *Gulick et al.* [1997] show that if surface temperatures increased from ∼220 K (present mean global temperature) to 240–250 K due to this effect, sublimation rates would increase rapidly and an ocean would sublimate completely in 10^3–10^4 years. Even though there are some uncertainties, *Gulick et al.* [1997] show that regardless of these, an ocean would persist for a very short time, shorter than any enhanced greenhouse effect.

2.3.2. Conversion to a Latitude-Dependent Ice Sheet

[39] The possible high sublimation rates cited above could lead to a rapid (∼0.1 Myr) reshaping of the frozen ocean to an ice sheet, rather than to its complete disappearance [see also *Kargel et al.*, 1995]. This timescale is comparable to the obliquity cycle [e.g., *Ward*, 1992]. Note that the long-term (∼10 Myr) chaotic obliquity variations [*Laskar and Robutel*, 1993] depend on the ice distribution, and this feedback makes it impossible to predict the climate conditions in the past [*Touma and Wisdom*, 1993; *Bills*, 1999]. Ice sublimed and redeposited in this way should no longer be considered as a frozen ocean. The present polar cap [e.g., *Thomas et al.*, 1992] with its finely layered structure, steep slopes, troughs, layered terrains, etc., shows an example of how evolved ice can look under Martian conditions. *Kargel et al.* [1995] modeled the option of glaciers evolving from seas which underwent progressive freezing, grounding, and sublimational redistribution of sea ice. They found that the transition to glaciation would have taken as long as several million years if the climate was comparable to that of Mars today.

2.3.3. Dynamic Effects of Outflow, Sublimation, and Redistribution

[40] The outflow events, as well as the sublimation and redistribution of the ice, mean that there is some redistribution of mass on the planet. The maximum possible change in the moment of inertia of the planet corresponds to a 1% relative change in the oblateness (gravity field spherical harmonic coefficient J_2). Such a change cannot have immediate catastrophic effects on the dynamics of Mars. Such changes would, however, definitely affect long-term obliquity variations (10 Myr and longer timescales) [*Touma and Wisdom*, 1993; *Bills*, 1999], although the chaotic nature of these variations do not permit the reconstruction of the obliquity history in the past regardless of our knowledge of variations of oblateness. *Bills and James* [1999] found that the rotation state of Mars is currently secularly unstable or close to the instability boundary. The mass redistribution treated here might affect the secular stability of the planet in the past, and influence a secular true polar wander, if it has ever occurred to a noticable extent.

2.3.4. Thermal Structure of the Frozen Ocean

[41] Since freezing of an ocean occurs from the surface to depth, the thermal anomaly caused by emplacement of water onto the surface would be actually relatively quickly buried by the formation of the ice sheet. This thermal anomaly would represent a somewhat higher temperature of the deeper parts of the ice sheet and upper parts of the cryosphere beneath the ice sheet, in comparison to the steady state geothermal gradient temperature distribution (segment 4 in Figure 5). As we saw above, when the cryosphere is thin (noticeably thinner than the water layer), temporal destruction of the cryosphere might occur. The thermal anomaly would exist for a period a few times longer than the freezing duration, that is, on the order of 0.1–1 Myr.

[42] After the thermal anomaly disappeared, the steady state geothermal gradient would be established (segment 5 in Figure 5). The layer of ice would work as thermal insulation, and the melting isotherm in the substrate (the cryosphere boundary) would be established at shallower depth below the floor than it used to be before the water emplacement. The thermal conductivity of ice is ∼1.7 times higher than that of the substrate. This means that when the steady state melting isotherm would reach the floor of the frozen ocean (that is the base of the ice sheet), the ice layer should be 1.7 times thicker than the cryosphere before water emplacement. This means, that the steady state conditions for melting at the base of the frozen ocean are even less probable then the temporal destruction of the cryosphere discussed in section 2.2.2.

[43] In the course of sublimation, the temperature of the ice (segment 6 in Figure 5) would follow the steady state geotherm, if the sublimation was slow, and would deflect from it for higher sublimation rates.

2.3.5. Outflow Events Over a Frozen Ocean

[44] A number of major outflow events happened in the Late Hesperian, a period of time estimated to be about 400–600 million years in duration, lasting from about 3.7/3.5 to 3.3/2.9 billion years ago [*Hartmann and Neukum*, 2001; *Ivanov*, 2001]. The question of whether or not the different outflow channels were generally synchronous and whether there were multiple events in single channels, is a matter of current debate (see discussion by *Carr* [1996a, 1996b]). There is evidence that some outflow channels apparently recorded more than one outflow event, and some of them are separated by geologically long time periods [e.g., *Tanaka*, 1997]. Thus, there is a distinct chance that an outflow event occurred after the water produced by the previous event froze and before it completely sublimed. The fate of water imposed on the surface of the frozen ocean could be somewhat different than that emplaced on deeply frozen ground.

[45] If the floodwater was warm, it would thermally erode the ice sheet. The heat brought by the warm water would be spent for melting the ice rather than for evaporation. Due to this, the warm ocean phase would be shorter.

[46] If the floodwater was cold, or after the water got cold, further melting of the underlying ice would occur. The ice would melt at the floor of the water layer and simultaneously the water would freeze at the lower surface of the ice sheet. The mechanism of this melting/refreezing process is similar to that which would drive the convection in the freezing ocean, but the melting at the floor works as a much more effective heat sink than the heat conduction to the frozen ground, and the process of the ice sheet growth goes much faster. In this fast process the rate of heat transfer

through the growing ice sheet and to the cryosphere is negligible in comparison to the rate of heat absorption and release during melting and refreezing. The internal energy of the floodwater would be also spent for heating of the portions of underlying ice to be melted from its initial temperature ($\sim T_s$) to the melting point T_0. This energy loss would be compensated by thinning of the water layer: freezing rate would exceed melting rate. The release of gravitational energy due to propagation of the denser water layer downward in the less dense ice layer is negligible, unless the water layer is less than $\sim$1 km thick. This process of melting at the bottom and refreezing at the ice sheet would go on, while the liquid water lasts or until all the ice is remelted. The thickness of ice that can be remelted is proportional to the thickness of the initial cold water layer and inversely proportional to $T_0 - T_s$. For $T_0 - T_s = 60$ K, for example, a 100 m thick layer of water can remelt a 300 m thick layer of underlying ice.

[47] Highstanding regions of ice would not be covered by newly-arrived water and would not undergo remelting. If the climate-driven volatile migration had produced a thicker ice sheet in the high-latitude region [e.g., *Kargel et al.*, 1995] (ultimately, a polar cap), the central part of such a sheet or polar cap would survive later outflow events. In this case the northern boundary of the ponded body of water would not follow the modern contour line. This mechanism could provide a thicker sediment layer in the peripheral parts of the northern lowlands.

2.3.6. Outflow Events Following Freezing and Sublimation

[48] If the previous body of water has frozen and completely sublimated, then new incoming outflow channel floodwaters will potentially erode and redeposit the sediment and sublimation residue resulting from previous outflow events. The complex stratigraphy of Chryse Planitia [e.g., *Tanaka*, 1997] may reflect some such activity, with later channels eroding and cutting into earlier deposits. Most Chryse outflow channels show a distinct change in the nature of their channel morphology at the margin of the basin over a short vertical range, although their detailed texture can be traced deeper into the basin [e.g., *Ivanov and Head*, 2001]. However, the youngest channel (Kasei 2 [*Tanaka*, 1997]), can be traced much deeper into the basin interior [e.g., *Ivanov and Head*, 2001; *Zuber et al.*, 2000; *Head et al.*, 2002; *Phillips et al.*, 2001], suggesting to us that as the last major outflow event into the North Polar Basin, it may have eroded into previous sedimentary deposits. Preferential erosion in the Chryse area may also be supported by the TES spectral signatures suggesting a higher percentage of blocks and bedrock than of fine-grained sediment [e.g., *Christensen*, 1986a, 1986b; *Bandfield et al.*, 2000; *Christensen et al.*, 2000].

[49] Emplacement of new floodwater could also cause partial ice melting and brine mobilization [see *Head and Pappalardo*, 1999, and references therein] in the ice-rich deposits left from the previous outflow events.

2.4. Final Fate of Water in the Ocean

[50] The final fate of the former ocean depends on where the water actually went. Several different fates or repositories are possible, including, freezing in place and preservation, sublimation, loss, transport, redeposition and drainage into the subsurface. We previously discussed sublimation rates. Sublimed water can follow several paths and almost all the water sublimed would finally condense somewhere on the surface. The fate of the frozen ocean strongly depends not only on sublimation, but also on condensation processes. Location of condensation strongly depends on the atmospheric circulation and is less dependent on the incident solar radiation pattern than the sublimation rate. The coldest regions on the planet (poles) are good candidates for areas of enhanced condensation; however it is not necessarily a requirement as shown by the situation on Earth, where condensation dominates in the warmest equatorial zone.

2.4.1. Frozen Remnant Ocean Layer

[51] *Clifford and Parker* [2001] proposed that a significant part of the water in ancient oceans underwent freezing, was covered with a sedimentary veneer before complete sublimation could occur, and is still preserved below the surface of the northern lowlands as layers many hundreds of meters thick. Our data, combined with that of *Head et al.* [2002], indicate little evidence for a thick layer of ice within the Vastitas Borealis Formation, or between it and the underlying Early Hesperian ridged plains. If any residual deposits remain in the northern lowlands from a proposed Noachian ocean [*Clifford and Parker*, 2001], they would lie below both the Vastitas Borealis Formation and the underlying sequence of Hesperian ridged plains.

2.4.2. Polar Caps

[52] The water ice that we see now on the surface of Mars is primarily concentrated in two polar caps. This ice can be the final fate of the water that went thorough the outflow events, probably after multiple sublimation — redeposition cycles. The total volume of the polar caps is about 3.2–4.7 $\times$ 10^6 km^3 [*Smith et al.*, 1999] which is $\sim$23–33% of the volume of the hypothesized northern lowlands ocean [*Parker et al.*, 1989, 1993] below contact 2 [*Head et al.*, 1999]. Thus, if the present polar caps represent the ultimate fate of the initial water, it can only account for a part of it, particularly since the polar deposits likely contain a significant dust component [e.g., *Thomas et al.*, 1992] or CO_2.

2.4.3. Ice-Rich Mantles

[53] Some water can be sequestered in the soil, in particular, the remnant sediments brought to the lowlands by the outflow events could still contain some ice. Evidence for a water-rich layer can be found in the latitude-dependent young mantle that is superposed on earlier geologic units [e.g., *Kreslavsky and Head*, 2000]. These young deposits may well contain ice [e.g., *Mustard et al.*, 2001], some of which may be related to redeposition of earlier bodies of water. The total volume of the ice that can be stored in these mantles is minor in comparison to the hypothesized ocean.

2.4.4. Deposition Elsewhere

[54] There is the possibility that there are some covered massive ice deposits on Mars outside the residual polar caps [e.g., *Schultz and Lutz*, 1988], or remnants of former ice deposits (e.g., the Dorsa Argentea Formation [*Head and Pratt*, 2001]). Condensation location strongly depends on atmospheric circulation and the coldest regions on the planet (poles) are good candidates for areas of enhanced condensation. The Hesperian-aged Dorsa Argentea Formation shows abundant evidence of areally extensive ice-rich deposits that may be related to the formation and fate of the

outflow channel effluents [e.g., *Head and Pratt*, 2001]. Condensation may also be influenced by local topography. *Head and Kreslavsky* [2001a, 2001b] have outlined evidence that some parts of the equatorial Medusae Fossae Formation may be condensation deposits from outflow channel deposit sublimation.

2.4.5. Drainage Into the Subsurface

[55] *Clifford* [1993] and *Clifford and Parker* [2001] hypothesized that accumulation of a thick layer of ice at the south pole could lead to melting of the ice at the base of the polar cap and the water could then drain into a deep subsurface aquifer. This process could provide an effective sink of water released in the outflow events. Our calculations and those of *Clifford and Parker* [2001] indicate that drainage into the subsurface directly from the ocean in the northern plains is not likely to occur.

2.4.6. Loss

[56] Some water certainly underwent photodissociation in the upper atmosphere and hydrogen escaped to space, while oxygen was bound by minerals. The total amount of the hydrogen escape is probably recorded in the isotope ratios, but we still cannot read this record unambiguously [e.g., *Owen*, 1992; *Pepin*, 1994; *Carr*, 1996a, 1999; *Leshin*, 2000; *Jakosky and Phillips*, 2001].

[57] On the basis of these observations, models and scenarios for evolution, we now assess the characteristics of the Vastitas Borealis Formation and compare these to the model predictions.

3. Vastitas Borealis Formation

3.1. Stratigraphic Position

[58] A variety of data show that the surface of the northern lowlands is flat and generally smooth at all scale lengths compared to terrains exposed elsewhere on Mars [*Smith et al.*, 1998; *Kreslavsky and Head*, 1999, 2000; *Aharonson et al.*, 1998; *Head et al.*, 1999]. About 45% of the northern lowlands are presently occupied by the Late Hesperian-aged Vastitas Borealis Formation [*Tanaka and Scott*, 1987; *Tanaka et al.*, 2002], which in turn is covered by the Early Amazonian-aged materials of the Elysium Formation in the Utopia Basin, the Arcadia Formation in Arcadia and Amazonis, and by Late Amazonian-aged polar and circum-polar deposits [*Scott and Tanaka*, 1986] (Figures 1 and 2). Prior to MGS, almost no tectonic structures had been detected in the northern lowlands [e.g., *Chicarro et al.*, 1985], but MOLA data revealed evidence for abundant wrinkle ridges there [*Head et al.*, 2002]. Superposition relationships described by *Head et al.* [2002] clearly show that a northern lowlands wrinkle-ridge system predates the Elysium Formation, the Arcadia Formation, and the present polar and circum-polar deposits. The topography of the wrinkle ridges is also observed in the Vastitas Borealis Formation, although in this unit ridge spacing tends to be greater and topographic expression more subdued than wrinkle ridges exposed elsewhere, suggesting that they are covered and subdued by the Vastitas Borealis Formation [*Head et al.*, 2002].

3.2. Roughness Characteristics and Nature of the Substrate

[59] Study of kilometer-scale roughness [*Kreslavsky and Head*, 2000] has shown that the Vastitas Borealis Formation is characterized by a distinctive dependence of roughness on scale. The dependence of the median differential slope used as a measure of roughness by *Kreslavsky and Head* [2000] on baseline length has a pronounced maximum at ~3 km baseline. Virtually no other terrains on Mars possess such a km-scale roughness signature. This characteristic 3 km-scale surface roughness is represented mostly by gently sloping knobs. This knobby pattern is partly undersampled in the gridded topography maps but still can be seen in 32 pixel-per-degree detrended topography images (Figure 6). Due to this specific texture, the boundaries of the Vastitas Borealis Formation are usually clearly seen in the detrended topography maps (Figure 6). The roughness map [*Kreslavsky and Head*, 2000] (Figure 1b) allows one to outline the boundaries even more reliably, but at lower resolution. In fact, at many locations, the topography and roughness maps enable one to outline the Vastitas Borealis Formation more reliably than the images. In some areas there are discrepancies between the boundaries seen in the roughness and topography maps and the boundaries mapped by *Scott and Tanaka* [1986] and *Greeley and Guest* [1987].

[60] Geological mapping shows that Hesperian ridged plains (Hr) are abundant in the uplands surrounding the northern lowlands [*Greeley and Guest*, 1987; *Tanaka and Scott*, 1987; *Scott and Tanaka*, 1986] and the stratigraphic columns in these maps place the Hesperian ridged plains (Hr) as Early Hesperian in age and the Vastitas Borealis Formation as Late Hesperian in age, essentially contemporaneous with the formation of outflow channels and their deposits (Figure 2). Stratigraphic evidence derived from the MOLA detrended data [*Head et al.*, 2002] strongly suggests that Hesperian ridged plains (Hr) underlie units presently exposed in the northern lowlands in Chryse Planitia, Acidalia Planitia and Utopia Planitia. This raises the question of whether the unusual roughness characteristics of the Vastitas Borealis Formation [*Kreslavsky and Head*, 1999, 2000] could be related to a combination of features associated with this unit and an underlying unit (Hr).

[61] To address this question, *Head et al.* [2002] examined the median differential slope of Hr exposed outside the northern lowlands and compared it to that of the Vastitas Borealis Formation. They found that Hesperian ridged plains are generally rougher than the Vastitas Borealis Formation, but the Vastitas Borealis Formation is very similar to Hr at intermediate scale lengths (2–5 km), and has lower differential slopes at shorter (<1 km) and longer (>8 km) scale lengths (Figures 7 and 8). Candidate processes for the origin of the Vastitas Borealis Formation include sedimentation and sedimentary redistribution processes, and so *Head et al.* [2002] modeled how thick a layer of overlying material would have to be to provide enough smoothing to make Hr appear like Hv.

[62] Using Hesperia Planum as a typical example of Hr, they found that for large patches of ridged plains, slopes at 80 km baseline still reflect the intrinsic surface roughness, while slopes at larger baselines are defined by regional topography. *Head et al.* [2002] used simulations of adding material to the typical Hr surface to find the minimum amount of material necessary to reach a given smoothness typical of the Vastitas Borealis Formation. Their simulations showed that application of a layer with a mean thickness of ~100 m can reduce the roughness from the level of Hr in

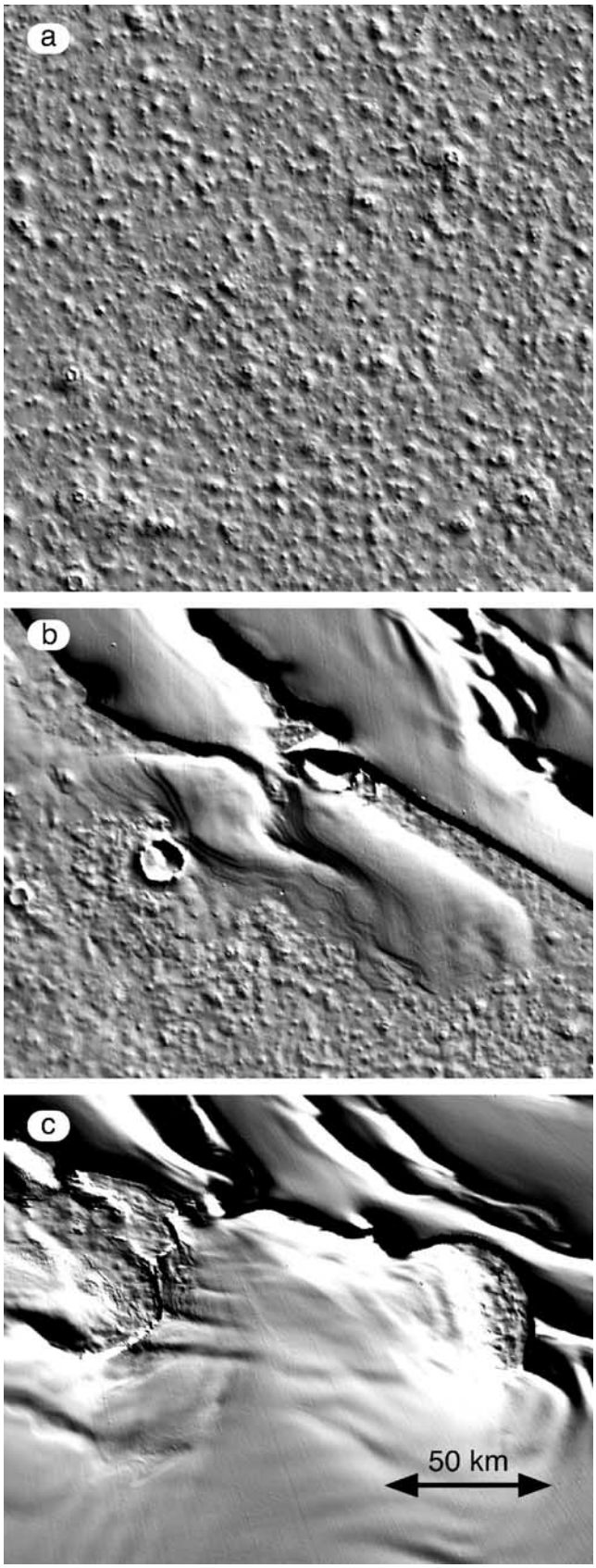

Figure 6. (opposite) The characteristic topographic pattern of the Vastitas Borealis Formation as seen in MOLA data. *Scott and Tanaka* [1986] originally described the Vastitas Borealis Formation (Hv) as subpolar plains deposits of the northern lowlands (Figure 1c), with four members distinguished on the basis of morphology or albedo contrast. The Mottled member (Hvm) is characterized by high-albedo deposits superposed on low-albedo smooth plains deposits; it is gradational with other members, particularly with Hvk. The Grooved member (Hvg) is marked by grooves forming curvilinear and polygonal patterns with polygons typically 5–20 km across. The Ridged member (Hvr) has concentric patterns of low, narrow ridges about 1–2 km wide, with the background material the same as that of Hvm. The Knobby member (Hvk) is characterized by abundant km-sized knoblike hills spaced a few km apart and often grouped into linear chains. The interknob areas are gradational with Hvm and Hvr. Cumulative densities of craters >5 km in diameter indicate that the Vastitas Borealis Formation is middle to late Hesperian in age [e.g., *Scott and Tanaka*, 1986] (see also Figure 2). The Vastitas Borealis Formation is locally mantled by circumpolar and polar deposits of Amazonian age [*Tanaka and Scott*, 1987; *Dial*, 1984] (see Figure 1c). (a) Shaded topography of a typical area of the Knobby member, Hvk. The scene is centered at 70°N 310°W, north is at the upper left. Knobby pattern is well sampled with MOLA data due to high shot density at high latitudes. Scale is the same as in (c). (b) Shaded topography of a contact between circumpolar mantling deposits (unit Am, lower part of the scene) and the polar cap deposits (upper part). The scene is centered at 78°N 0°W, north is at the top, the scale and contrast are the same as in (a) and (c). The circumpolar mantling displays the same knobby pattern as Hvk in (a). This pattern can be seen in the floor of troughs of the polar cap. (c) Shaded topography of the northern part of Chasma Boreale within the polar cap. The scene is centered at 84°N 5°W, north is at the top, and the scale and contrast are the same as in (a) and (b). The characteristic knobby pattern is seen in the deepest parts of the canyon. (d) Shaded topography of a typical area of the Grooved member, Hvg, in Utopia Planitia. The scene is centered at 37°N 257°W, north is at the top. (e) Detrended topography obtained with a high-pass median filter with a circular core of a diameter of 40 km for the same area. Brighter shades denote locally higher elevations. Grooves are undersampled in MOLA data. A contact with the Elysium Formation is clearly seen in the eastern part of the scene. (f) Shaded topography of a typical area of the Ridged member, Hvr, in northern Arcadia Planitia. The scene is centered at 57°N 174°W, north is at the top, the scale is the same as in (d) and (e). (g) Detrended topography obtained with a high-pass median filter with a circular core of a diameter of 100 km for the same area. Ridges are undersampled in MOLA data. It is well seen that the small subparallel ridges forming a whorl-like pattern are modulated by a wide smooth ridge-like high in the center of the scene; however, the ridges do not follow contour lines. This behavior is consistent with the interpretation of ridges as recessional moraines. A contact with the Arcadia Formation is seen in the southeastern part of the scene.

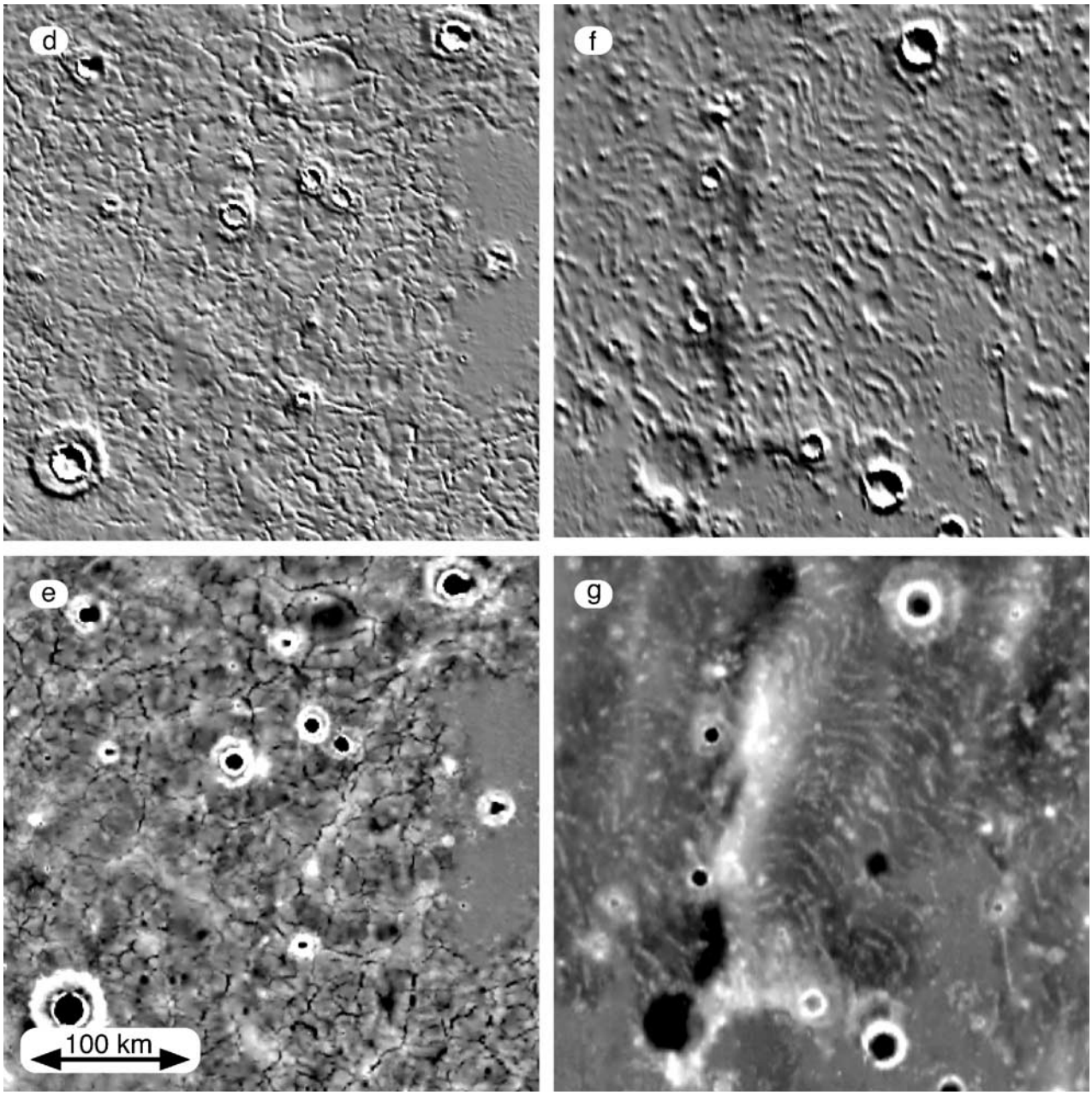

Figure 6. (continued)

Hesperia Planum to the level of the Vastitas Borealis Formation. The resulting average thickness of 100 m provides a lower boundary for the mean thickness of the Vastitas Borealis Formation material. The mean thickness can be higher, because the emplacement may differ from the effective smoothing algorithm. Local thickness of the Vastitas Borealis material may vary over a wider range.

[63] The detrended data also revealed a large number of circular features with a range of diameters and a very subdued morphology (Figures 9 and 10) which *Head et al.* [2002] interpreted as hidden, or "stealth," circular depressions, representing subdued and buried impact craters formed on a surface of Early Hesperian age. They thus concluded that on the basis of stratigraphic relations and surface roughness analyses, the Vastitas Borealis Formation could plausibly represent a thin veneer of about 100 m minimum thickness superposed on Hesperian ridged plains (Hr) in the northern lowlands (Figure 7).

3.3. Relation to Outflow Channel Deposits

[64] Contemporaneous with the Late Hesperian Vastitas Borealis Formation are the Late Hesperian channel deposits (Hc), representing the formation of the outflow channels and their debouching into the northern lowlands (Figure 2). The detailed nature of these outflow events is controversial (e.g., see review by *Carr* [1996a, 1996b]), but all agree that their formation involved emplacement of sediment into the northern lowlands. *Carr et al.* [1987] estimated that around the Chryse basin (the area of the most significant channel input into the northern lowlands), the volume of sediment

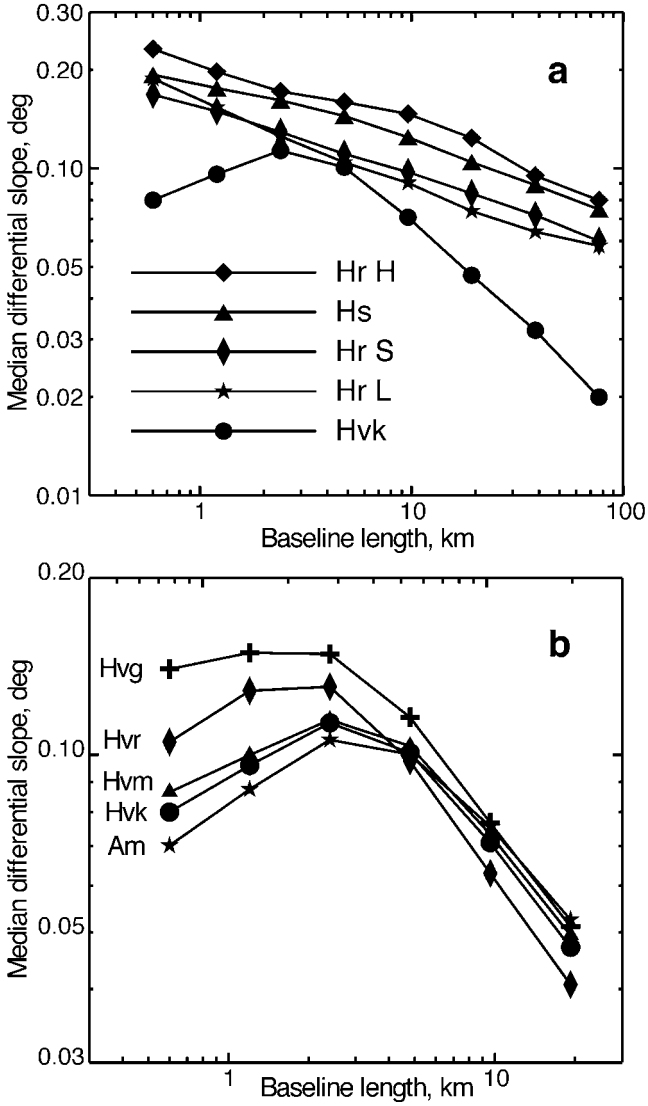

Figure 7. Vastitas Borealis Formation roughness characteristics and comparison to those of Hesperian-aged ridged plains. Shown is the dependence of the median absolute value of differential slope on the baseline length (logarithmic scale on both axes). The median absolute value of differential slope for a given baseline length characterizes the surface roughness at the spatial scale of the baseline length (see *Kreslavsky and Head* [2000] for details). (a) Comparison of a typical Vastitas Borealis Formation roughness signature (Knobby member, Hvk) with a number of ridged plains units: Hs, the Syrtis Major Formation; Hr L, Lunae Planum; Hr S, the eastern part of Sinai Planum; Hr H, Hesperia Planum. (b) Comparison of the northern plains units. Am, circumpolar mantling deposits. Vastitas Borealis Formation members: Hvk, Knobby; Hvm, Mottled; Hvg, Grooved; Hvr, Ridged. Unit boundaries are taken from 1:15,000,000 USGS geological maps of Mars [*Scott and Tanaka*, 1986; *Tanaka and Scott*, 1987; *Greeley and Guest*, 1987]. Note that the Vastitas Borealis Formation members are typically smoother than Hr (ridged volcanic plains) at the range of scale lengths. See Figure 1c for areal distribution of subunits.

eroded from the channels and collapse features and emplaced into the lowlands was about 4×10^6 km^3. *Head et al.* [2002] pointed out that if the Vastitas Borealis Formation represents a sedimentary unit emplaced over the northern lowlands with a minimum average thickness of about 100 meters, then its minimum total volume would be about 3×10^6 km^3, in general agreement with Carr's 4×10^6 km^3 estimate of the amount eroded. On the basis of these several considerations, it seems plausible that the Vastitas Borealis Formation represents at least part of a sedimentary layer emplaced during outflow channel formation. If true, then the nature of the substrate, the deposit itself, and its relation to subsequent deposits, may provide additional clues to the mode of formation of the outflow channel deposits and their fate. In the following sections we address these issues.

3.4. Nature of Impact Craters on the Substrate

[65] The large number of subdued circular features ("stealth" craters) revealed in the detrended topography data and lying on the ridged plains below the Vastitas Borealis Formation (Figures 9 and 10) may provide evidence on the emplacement process of that unit. For example, if some craters were totally erased by emplacement of the Vastitas Borealis Formation, we would expect that smaller craters would be more likely to be erased than large craters; hence, we should find a noticable relative paucity of small stealth craters. *Head et al.* [2002] compared the nature of craters below the Vastitas Borealis Formation ("stealth") to those superposed on it. The size-frequency distribution of the stealth craters turned out to be remarkably similar to that of the superposed craters (Figure 9), and thus it is probable that almost all craters above about 15 km that formed on the substrate before or during the emplacement of the Vastitas Borealis Formation are preserved.

[66] What information is provided by the morphometry and morphology of the stealth craters? *Head et al.* [2002] measured the depth of the craters as the difference between the elevation of the surroundings and the elevation of the crater floor (Figure 9). The depths of fresh craters are scattered, with larger craters generally deeper. Stealth crater depths are scattered around 100 m, and no dependence of depth on crater size is observed. Only two stealth craters are deeper than 200 m, one of them being the largest stealth crater. This observed very shallow nature of stealth craters is consistent with their extensive erosion and infill after their formation on an underlying unit, interpreted to be Hesperian ridged plains [*Head et al.*, 2002], while the depth distribution of the fresh craters suggests that they have not undergone the same level of erosion and infilling. In summary, *Head et al.* [2002] conclude that the contrast in crater depths between these two populations suggests that the stealth craters underwent modification and shallowing during Late Hesperian, coincident with the emplacement of the Vastitas Borealis Formation.

[67] If we assume that the two crater populations (pre- and post-Vastitas Borealis Formation) are approximately the same in size frequency distribution (as indicated by the data; Figure 9) and that the post-VBF population is similar to other fresh craters in morphology and morphometry, as indicated by comparison to the data of *Garvin et al.* [2000a, 2000b], then the differences in characteristics can

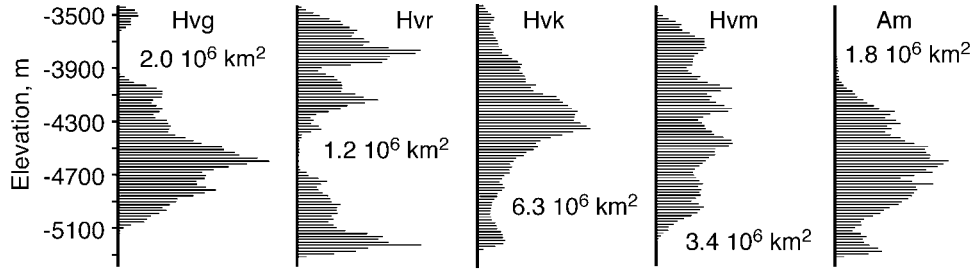

Figure 8. Distribution of elevations of the northern plains geological units. Am, circumpolar mantling deposits. Vastitas Borealis Formation members: Hvk, Knobby; Hvm, Mottled; Hvg, Grooved; Hvr, Ridged. Unit boundaries are taken from 1:15,000,000 USGS geological maps of Mars [*Scott and Tanaka*, 1986; *Tanaka and Scott*, 1987; *Greeley and Guest*, 1987]. The elevation histograms are normalized by the total area of each unit, which is also shown. See Figure 1c for areal distribution of subunits.

be used to assess modification processes. Differences between the average depths (Figure 9) could be explained by the deposition in the interiors of from a few hundred meters for smaller craters up to ~1000 meters for larger pre-VBF craters during the emplacement of the VBF. Lava flooding by late-stage Hr could be partly responsible, but flooding usually causes breaching and near-complete eradication, and the morphology of these craters (Figure 9) is not similar to flooded craters seen elsewhere. Another possibility is that rapid outflow of water into the lowlands during channel formation events eroded sediment from the impact crater rims and deposited it into the crater interior. Examination of typical stealth craters (Figure 9) shows that their rims are generally very narrow and subdued relative to the well-developed and laterally extensive ejecta deposits of younger craters. Analysis of the volumes of fresh crater ejecta deposits [*Garvin et al.*, 2000a, 2000b] shows that this material alone is capable of filling the crater depression. We also examined the distribution of stealth craters (Figure 10) and found that they were relatively evenly distributed, but with fewer in the deepest parts of the North Polar Basin. We found no significant correlations when we plotted the distribution and size of stealth craters as a function of elevation, and size as a function of areal distribution.

[68] Another process of modification to produce stealth craters could be viscous relaxation of crater rims and interiors due to their formation in a substrate with an upper layer of ice several hundreds of meters thick (the frozen ocean). In this scenario, ice might be abundant in the upper part in the ejecta deposit and substrate, and thus any crater formed in this substrate would undergo modification processes that could produce loss of volume due to sublimation and possible melting, and viscous relaxation and creep due to properties of the ice-rich layer. If, as envisioned by *Carr* [1996a, 1996b], some frozen floodwater could have reached thermal and diffusive stability due to a thin cover of sediment or lavas, then such a layer might have been present for a long period of time and might even have persisted until today. Indeed, *Clifford and Parker* [1999, 2001] concluded that the presence of such massive ice deposits beneath the northern plains was consistent with a variety of observations, including their smoothness and geomorphology of landforms. The results and interpretations reported by *Head et al.* [2002], however, do not favor the hypotheses of massive ice deposits beneath the northern lowland surface. If thick frozen residues of the outflow channel floodwaters existed in the northern lowlands, they should largely bury underlying topography. However, the detected presence of the underlying Early Hesperian plains, stealth craters, and wrinkle ridges, suggest that any layer overlying these plains must be very thin, less than a few hundred meters in thickness. As we discussed, a more likely explanation is that the overlying material is the Vastitas Borealis Formation, composed of the sedimentary residue of the sediment/water effluent of the outflow channels. If any residual deposits remain in the northern lowlands from a proposed Noachian ocean [*Clifford and Parker*, 2001], they would lie below both the Vastitas Borealis Formation and the underlying sequence of Hesperian ridged plains. In summary, although viscous relaxation could potentially operate during the presence of an ice layer, the duration of the ice layer seems to be sufficiently short that only a small number of impacts would have formed. Similarly, impact into a standing body of water [e.g., *Lindstrom et al.*, 1996], which might involve catastrophic backwash, tending to cause erosion of the rims and infilling of the interior, could operate under very special circumstances, but the period of time liquid water would be stable on the surface would be so short [e.g., *Carr*, 1996a; *Gulick et al.*, 1997] that it is unlikely to provide an explanation for the large number of stealth craters.

[69] Other processes might include glacial planing [e.g., *Kargel et al.*, 1995] during evolution of the ice sheet, which might remove the rim and infill the crater, and eolian redistribution of sediment. Both these processes, however, would have to operate preferentially on the stealth craters, because younger craters formed on the surface of the Vastitas Borealis over the last several billion years have not been affected in the same manner. Finally, significant crater modification of stealth craters might have occurred due to discharge of water from the subsurface under high artesian pressure soon after the impact, as described by *Clifford and Parker* [2001]. Craters superposed on the VBF, however, do not display any signs of associated hydrologic activity [e.g., *Russell and Head*, 2002].

[70] On the basis of the characteristics of the stealth craters and the discussion of the range of processes, we conclude that the most likely processes of modification are erosion and deposition associated with the emplacement of the outflow channels effluent, which should degrade the rims and infill the crater interiors, and additional processes of sedimentation during the freezing of this layer. Extreme

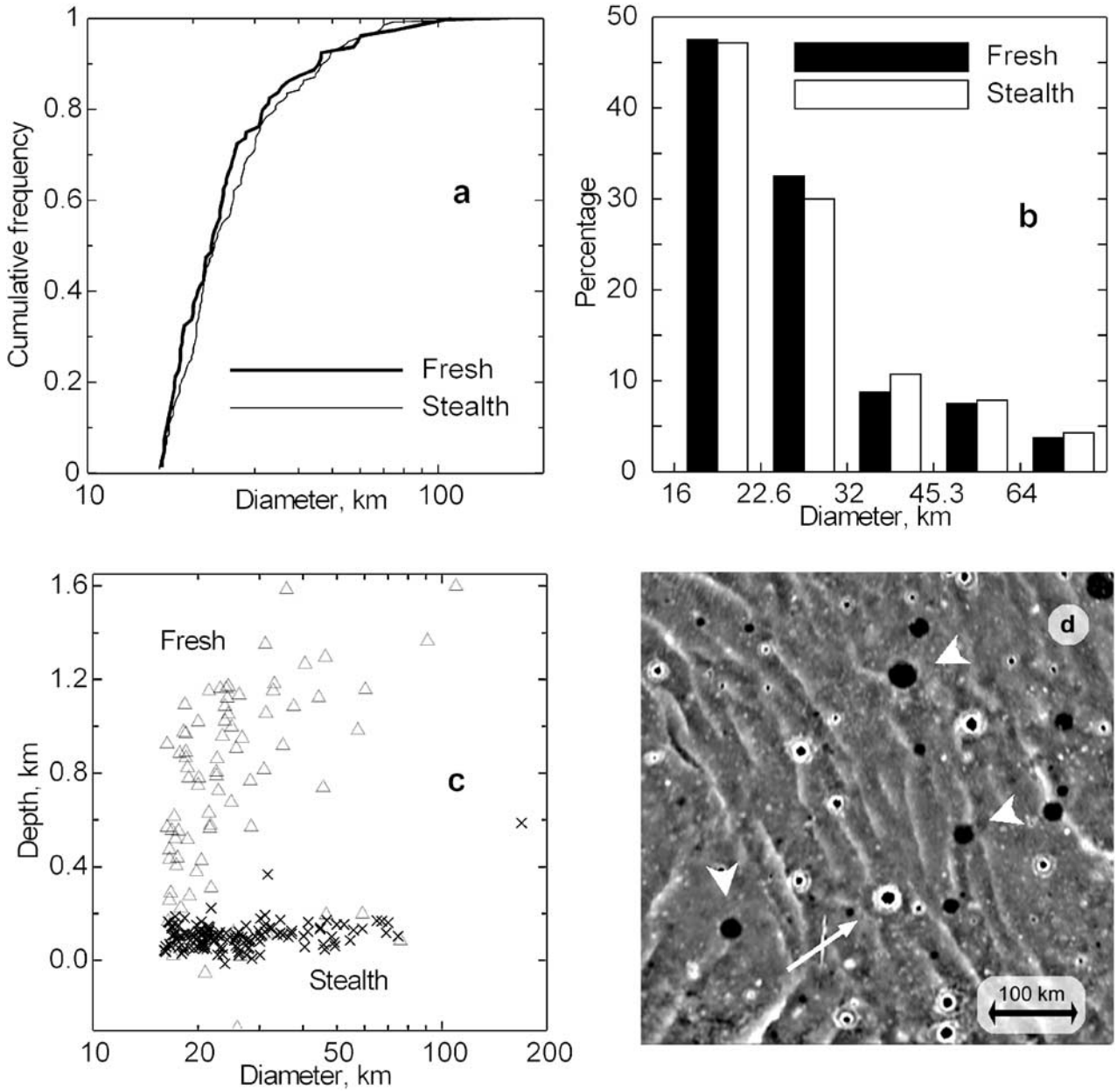

Figure 9. Comparison of "real" craters (interpreted to be superposed on the Vastitas Borealis Formation on the basis of their crisp morphology) and "stealth" craters (interpreted to be overlain by the Vastitas Borealis Formation on the basis of their very subdued morphology). (a) Cumulative diameter-frequency distribution for stealth craters (narrow line) and superposed (real) craters (thick line) within the Vastitas Borealis Formation outline (excluding Isidis basin). (b) Diameter frequency of stealth and superposed (real) craters for a conventional set of diameter bins. (c) Depth-diameter relationships of stealth craters (x's) and superposed (real) craters (triangles). (d) Detrended topographic map (100 km filter core radius) showing numerous examples of stealth (dark) and real (brighter) craters. The scene is centered at 65°N, 223°W, and north is at the top.

sedimentation rates of 50 cm per year are known in terrestrial submarine craters [e.g., *Thatje et al.*, 1999]. An additional factor in the shallowing of the craters could be the preservation of ice in the crater interiors. Although we have not found compelling evidence for the preservation of thick widespread layers of ice preserved below an insulating sedimentary layer, as envisioned by *Clifford and Parker* [1999, 2001], nonetheless, such an environment might be expected to occur preferentially inside impact craters that are flooded by outflow channel effluent (Figure 11). Thus, one of the best candidates to sample remnants of Hesperian oceans might be below these crater floors.

3.5. Distribution and Interpretation of Vastitas Borealis Formation Subunits

[71] *Scott and Tanaka* [1986] originally described the Vastitas Borealis Formation (Hv) as subpolar plains deposits of the northern lowlands, with four members distinguished

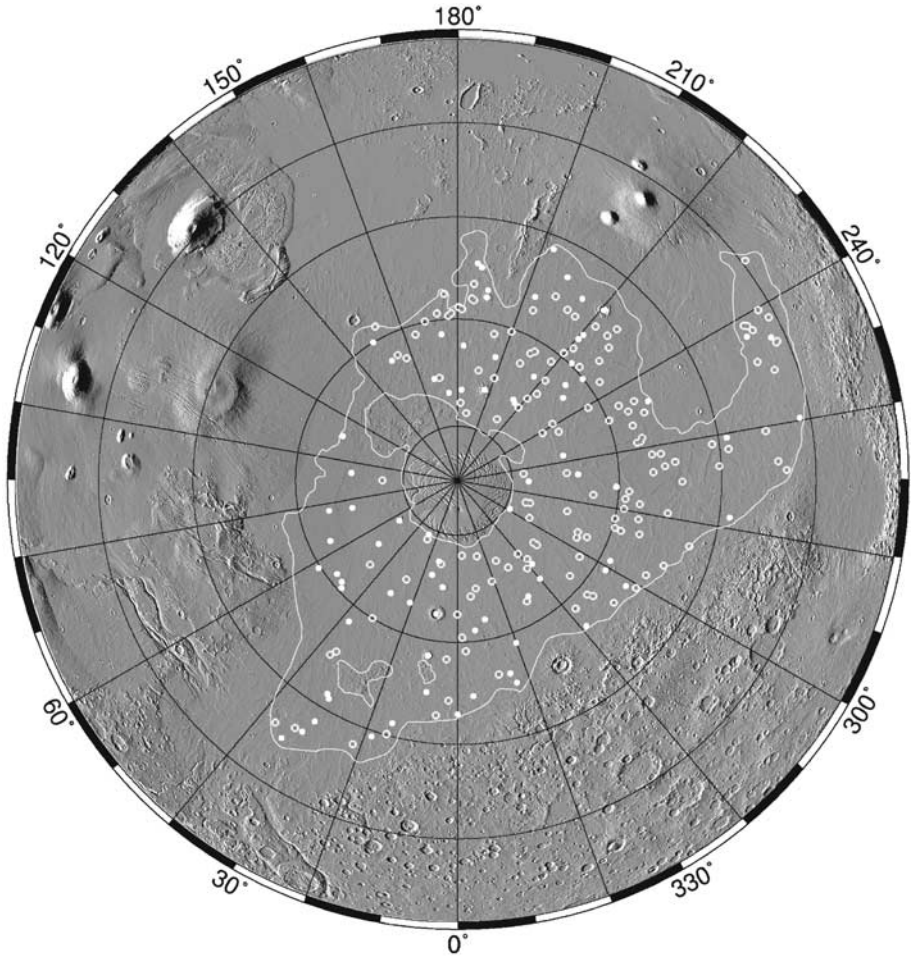

Figure 10. Areal distribution of stealth craters (open circles) and superposed (real) craters (solid circles) within the Vastitas Borealis Formation (as outlined). The background is the simulated shaded topography map of the northern hemisphere. Compare to Figure 1.

on the basis of morphology or albedo contrast (Figure 6). We concur with *Tanaka et al.* [2002] that subunits of Hv are not sharply defined units that can be distinguished stratigraphically with superposition relationships, and we refer to them as members or facies. The Mottled member (Hvm) is characterized by high-albedo deposits superposed on lower-albedo smooth plains deposits; it is gradational with other members, particularly with Hvk. The mottled appearance was noted to be commonly associated with bright impact craters and their ejecta, and was considered to be due either to light-colored material exposed during impact or to high-albedo eolian debris trapped in crater ejecta. The unit itself

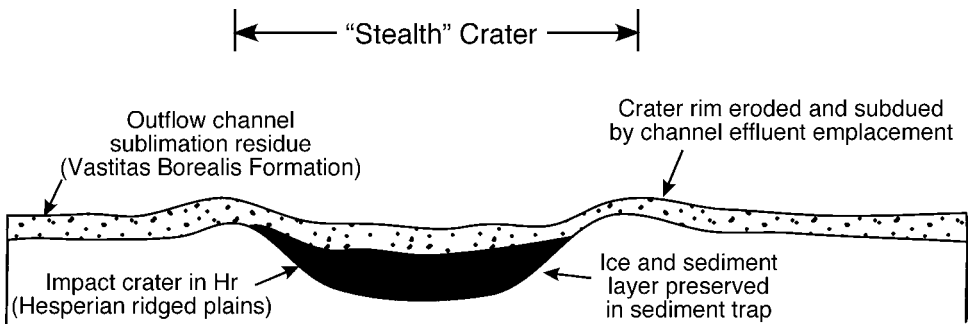

Figure 11. Cross-sectional portrayal of a stealth crater with a possible ice and sediment fill and sediment cover. Filling of the crater during emplacement of outflow channel effluents could have led to concentration of water-rich sediment and the evolution of a sediment cover during sublimation could have preferentially protected the ice-rich sediment in the bottom of the crater for significant periods of time, perhaps even until today.

was interpreted as lava flows, alluvial, or eolian deposits. The Grooved member (Hvg) (Figures 6d and 6e) is marked by grooves forming curvilinear and polygonal patterns with polygons typically 5–20 km across. Material is thought to be the same as that of the Hvm, but modified differently to produce polygons. The Ridged member (Hvr) has concentric patterns of low, narrow ridges about 1–2 km wide, with the background material the same as that of Hvm. The Knobby member (Hvk) is characterized by abundant km-sized knoblike hills spaced a few km apart (Figure 6a) and often grouped into linear chains. The interknob areas are gradational with Hvm and Hvr. The unit occurs in a broad circumpolar belt and the knobs are interpreted by *Scott and Tanaka* [1986] and *Tanaka and Scott* [1987] as small volcanoes and highly degraded members of highland material units and underlying crater rims.

[72] We used MOLA data to examine the Vastitas Borealis Formation and its subunits in terms of latitude and altitude distribution and roughness characteristics. We used interpolated topography and the geological maps to obtain the hypsometric distribution of the members of the Vastitas Borealis Formation, and Figure 8 shows these distributions normalized to the total area of each member. Hvk, the knobby member, comprises almost half of the area of the unit. Its mean elevation (−4300 m) is close to the mean elevation of the unit as a whole (−4340 m). Hvg, the grooved member, tends to occupy lower elevations, with a mean elevation of −4510 m. Hvr, the ridged terrain has a well-pronounced bimodal hypsometric distribution with ridged units occupying both the lowest and highest parts of the Vastitas Borealis Formation. Hvm, the mottled member, has the same mean elevation distribution as Hvk, but its hypsometric distribution is much wider, being relatively evenly distributed over the whole altitude range. Its areal distribution, however, is largely toward the edge of the basin from Hvk. Also shown in Figure 8 is the hypsometric distribution of the superposed Amazonian-aged circumpolar mantling deposits (Am), which have a mean elevation of −4620 m, similar to that of the grooved member (Hvg).

[73] The concentration of the Grooved member (Hvg) in the lower parts of the northern lowlands is consistent with the large grooves and polygons being related to the presence of former standing bodies of water (e.g., unloading, etc. [*Hiesinger and Head*, 2000]). The concentration of the Ridged member (Hvr) at elevations in the upper part of the basin (upper peaks) could be consistent with these representing shoreline [*Parker et al.*, 1989, 1993] or ice [*Carr and Schaber*, 1977; *Kargel et al.*, 1995] retreat, although this does not explain the lowest peak. The Knobby member (Hvk) is concentrated in the upper part of the basin, and this is in part due to the presence of degraded knobs of highland material there, partly destroyed and buried by the emplacement of Vastitas Borealis Formation and other units. Parts of this unusual terrain could also be related to dewatering of the substrate during a recessional phase (in the form of mud volcanoes and or pingos) [*Head et al.*, 2001]. The Mottled member (Hvm) is relatively evenly distributed as a function of elevation. If the albedo of the craters representing the mottling is due to excavation of a different substrate, the material could plausibly represent fine-grained clastic or evaporitic sedimentation lying below a thin eolian mantle. High resolution spectral data for these ejecta deposits should provide tests for this possibility.

[74] We previously described the roughness characteristics of the unit as a whole [*Kreslavsky and Head*, 1999, 2000; this article], and here we show the relationship of the subunits to each other and to the Amazonian mantling deposits (Am) (Figure 7). The scale dependence of roughness is remarkably similar for all members of the Vastitas Borealis Formation. The maximum differences between units are about a factor of two and occur at the shortest baseline. All of the subunits show a characteristic scale of surface slope (about 3 km) and very similar slopes at longer baselines. This suggests similar origins of the gentle background topography with a characteristic slope length of about 3 km and slope steepness of about 0.3° [e.g., *Kreslavsky and Head*, 1999].

[75] Units Hvk and Hvm display the same roughness at all scales, suggesting that the characteristic impact crater albedo pattern of the mottled subunit is formed by thin ejecta deposits that are not seen in topography at this scale. The differences in roughness in Hv subunits at the shorter baselines may be due to several factors. For example, the grooves associated with Hvg are commonly linear and vertically pronounced (several tens of meters; see *Hiesinger and Head* [2000]). Similar characteristics are seen for the ridges in Hvr. The knobs of the knobby member differ regionally in their abundance within the unit, and even where they are abundant, the knobs themselves occupy only a small percentage of the total area of the unit. Their density and equidimensional nature, in contrast to the linear nature of Hvg and Hvr grooves and ridges, means that MOLA profiles will tend to undersample the knobs. Thus, Hvm, with fewer linear grooves and ridges, is more similar to Hvk, than it is to Hvg and Hvr. The latitudinal trend of small-scale roughness seen in the roughness data, and apparently due to a thin, very young mantling unit [*Kreslavsky and Head*, 2000] may be another factor, as a significant part of the grooved terrain is in Utopia Planitia, at latitudes generally below this effect.

[76] In summary, the Vastitas Borealis Formation is characterized by a generally very similar smoothness at intermediate to longer scale lengths (Figure 7) and is similar in smoothness to younger sedimentary mantling material (Am) (Figure 6b). Differences at shorter scale lengths seem to be plausibly related to differences in the morphology of the individual members and to latitudinal variations. We return to the interpretation of the distinctive and unusual characteristics of the Vastitas Borealis Formation and its subunits in the discussion section.

4. Discussion and Conclusions

4.1. Channel Effluent Emplacement and Fate of Volatile Species

[77] Outflow channel effluents consisting of water, sediments and released CO_2 were emplaced into the northern lowlands during the Hesperian. Most evidence suggests that the temperatures and pressures of the Martian atmosphere during this time were much more similar to what they are today than ''warmer and wetter'' conditions hypothesized to exist in the earliest history of Mars (Figure 5). Under this very plausible and likely range of conditions, the inevitable

fate of the water emplaced into the northern lowlands is very rapid freezing solid of ponded water deposits. The rate of ice sublimation is not well constrained. The minimum residence time of the volatiles associated with the outflow channel effluents thus seems likely to be of the order of a few hundred thousand years, or even shorter (Figures 4–5). Formation of temporary atmosphere effects from significant additions of CO_2 during the initiation and emplacement of outflow channels would accelerate the rate of sublimation of the remaining ice [e.g., *Gulick et al.*, 1997]. Covering of the solid ice with a veneer of sublimation-inhibiting sediments could theoretically prolong the presence of the ice indefinitely [e.g., *Carr*, 1996a], even to the present [e.g., *Clifford and Parker*, 2001]. However, examination of the stratigraphy of the northern lowlands shows no evidence for the presence of such a layer today, nor any evidence that such a layer existed in recent geological epochs.

4.2. Vastitas Borealis Formation

[78] The Late Hesperian Vastitas Borealis Formation is an unusual and unique unit occurring in the northern lowlands and on the Isidis Basin floor and nowhere else on Mars. Stratigraphic analysis supports the interpretation that it is superposed on Hr, the Early Hesperian ridged plains of volcanic origin. A variety of evidence (roughness properties, conversion simulations from Hr to Hv, occurrence and nature of stealth craters, etc.) indicates that the Vastitas Borealis Formation has a minimum average thickness of about 100 meters. Thus, the Vastitas Borealis Formation, previously defined as a regional unit of complex origin [e.g., *Scott and Tanaka*, 1986; *Tanaka and Scott*, 1987], is now seen as a thin sedimentary unit overlying volcanic plains [e.g., *Head et al.*, 2002]. Ages and stratigraphic relations support the interpretation that the Vastitas Borealis Formation is laterally equivalent to the outflow channels (e.g., formed contemporaneously) (Figure 2) and that the unit represents the deposits remaining from outflow channel emplacement events.

4.3. Interpretation of the Vastitas Borealis Formation

[79] On the basis of the characteristics of the Vastitas Borealis Formation and its subunits, we interpret the unit to be the sedimentary residue of sediment-laden water emplaced during outflow channel formation. The relatively even distribution and thickness of the unit can be accounted for by much of the sediment being carried in suspension and deposited during Phase 1, the warm ocean phase. During this phase, the violent emplacement of ''warm'' water was followed by a short period of intensive evaporation and intensive convection in which the water maintained and redistributed its large suspended sediment load; when intensive convection ceased, the water deposited the suspended sediments. This short period, when the water is a few degrees above the freezing point of the point of maximal density, is essential to explain the absence of the massive deposits near mouths of the outflow channels. During Phase 2 (the freezing phase) rapid freezing of the water body was accompanied by weak convective water movement over a period of the order of $\sim 10^4$ years.

[80] The major morphological subunits of the Vastitas Borealis Formation, Hvg, Hvr, and Hvk, are reinterpreted in this context. The very large size of the grooves, troughs and polygons constituting the Hvg subunit (Figure 6), and their hypsometric distribution (predominantly in the lower, and thus deeper parts of the lowlands) (Figure 8), are interpreted to mean that these formed due to unloading and deformation following the removal of the water load [e.g., *Hiesinger and Head*, 2000]. On the basis of the stratigraphic relationships, it is clear that in the Utopia Basin, these features cut the Vastitas Borealis Formation, but are covered by the Early Hesperian deposits of the Elysium Formation [e.g., *Tanaka et al.*, 1992; *Hiesinger and Head*, 2000; *Thomson and Head*, 2001; *Russell and Head*, 2001].

[81] The whorl-like ridge patterns that characterize the Hvr subunit (Figure 6) occur predominantly in the higher parts of the basin near the edge of the Vastitas Borealis Formation (Figure 1c; Figure 8). We interpret these to be related to Phase 3, sublimation and loss of the ice layer. We concur with *Kargel et al.* [1995] in their comparison of these features to recessional moraines. Their occurrence predominantly at high elevations near the margins of the ice layer is consistent with lateral, as well as vertical shrinkage of the ice sheet.

[82] The ubiquitous knobs characteristic of the Hvk subunit are likely to have multiple origins. Those near the boundary with the ancient highlands include features that are degraded remnants of this terrain, as attested to by the circular arcs of knobs that are candidates for heavily degraded impact crater rims. Also near the edge of the basin are numerous lava flow units associated with Tharsis and Elysium. Recent documentation of volcanic pseudocraters in high-resolution MOC images [e.g., *Lanagan et al.*, 2001] in the Elysium and Amazonis region supports the interpretation of rootless cones formed by lava flowing over water-rich substrates for at least a subset of the knobs. Detailed analysis of individual groups of these features in MOC images [e.g., *Head et al.*, 2001] will be required to assess whether the knobs documented by *Frey and Jarosewich* [1982] are also of pseudocrater origin. A variation on this theme may be the eruption of lavas below the ice surface at the sediment/ice interface. Although this option has not been proposed for the Hvk knobs, analysis of the theory of subglacial eruptions [*Wilson and Head*, 2002] suggests that it may occur locally.

[83] Other interpretations may be related to the evolution of the water body during Phase 2, when it freezes, or during Phase 3, when the solid ice substrate sublimes. During Phase 2, freezing fronts will be proceeding from both the base and top of the water body. Increased pressure during this phase (e.g., expansion associated with freezing, overlying weight of ice) could produce an overpressured liquid layer and form pingo-like features or even mud volcanoes if sediment were involved. This could result in a series of knobs in the diameter range of meters to hundreds of meters [e.g., *Head et al.*, 2001]. Further sublimation might destroy the evidence of these unless they included significant admixtures of sediments.

[84] Phase 3, during the sublimation of the ice sheet, is the most likely time of formation of these features because if this process is indeed operating to form the Vastitas Borealis Formation sediment layer, then the surface should represent the last stages of its evolution. A process similar to that described during Phase 2, extrusion of melt, could also operate during Phase 3 if there were pockets of

concentrated brine that might have escaped freezing and been extruded to the surface with sediments. A second possibility is that some knobs simply represent the remnants of heterogeneous sublimation, with sublimation being more complete in areas of more pure ice, and less complete in areas of ice with sedimentary impurities. Examination of decaying glaciers on Earth offers some instructive examples. Kame and kettle topography is typical of decaying glaciers. Kames form tracts of mounds and ridges composed of masses of glacifluvial deposits between intervening lows representing areas of subsidence caused by melting of buried ice [*Benn and Evans*, 1998]. Further redistribution and concentration of sediment and silicate substrate material by impact cratering at all scales could also influence the distribution of knob-like topography. For example, ejecta deposits could armor ice patches, producing concentrations of sedimentary debris.

[85] The origin of the distinctive background 3-km scale topographic roughness characteristic for the whole Vastitas Borealis Formation is not perfectly clear. Knobs discussed above contribute to this roughness signature, but do not define it. The background 3-km scale topographic pattern might be due to sediment redistribution and/or salt deposits produced by the networks of stable eddies in the freezing ocean, as it was described in section 2.2.3.

4.4. Mineralogy and Petrology of the Northern Lowlands

[86] *Bandfield et al.* [2000], using Thermal Emission Spectrometer (TES) data, identified two distinctive terrains on Mars. Type 1, which they interpreted to be basaltic in nature, is found throughout the southern highlands. Type 2, which they interpreted as basaltic andesite, is concentrated in the northern lowlands. *Bandfield et al.* [2000] concluded that there was a fundamental difference in the mineralogy of the two terrain types and that this might imply a basic difference in the petrogenetic origin of the terrains.

[87] *Noble and Pieters* [2001] pointed out that basaltic weathering might provide an alternative interpretation of the spectral characteristics of Type 2 terrain, suggesting that a larger glass component in Type 2 terrain could cause the difference from Type 1 spectra, and that this additional glass component could come from basaltic weathering, as opposed to fundamental petrogenetic differences. *Wyatt et al.* [2002] developed multiple working hypotheses for the distribution of these surface materials, and concluded that Type 2 material might represent either (1) an influx of basaltic sediment from the southern highlands deposited on andesitic volcanics, or (2) incompletely weathered basalt marking the geographic extent of submarine alteration of basaltic crust.

[88] Our work strongly supports these alternative interpretations. *Head et al.* [2002] showed that the material underlying the Vastitas Borealis Formation is very likely to be Hesperian-aged ridged plains, laterally correlative with the Hesperian ridged plains widely distributed in the southern uplands and identified by *Bandfield et al.* [2000] to be Type 1 basaltic terrain (for example at Syrtis Major). In this work we show that the surface unit making up the majority of the Type 2 terrain, the VBF, is composed of sediment derived from the southern uplands, terrain typical of Type 1 basalts of *Bandfield et al.* [2000]. Thus, we concur with the multiple working hypotheses of *Wyatt et al.* [2002] and suggest a further definition of the possibilities: (1) an influx of weathered basaltic sediment from the southern highlands deposited on basaltic volcanics (the underlying Hesperian ridged plains [*Head et al.*, 2002]), (2) incompletely weathered basalt marking the geographic extent of submarine alteration of basaltic crust due to the interaction of the floodwaters with underlying basalt, or (3) a combination of these (transport of weathered basalt from the southern uplands and further alteration of the basaltic sediments and substrate during the residence time of the water). All three of these alternatives agree with the work of *McSween* [2002] that the crust of Mars is largely basaltic in nature.

4.5. Tectonic Response of the Northern Lowlands to Volcanic Loading, Outflow Channel Effluent Emplacement, and Volatile Loss

[89] Transfer of material across planetary surfaces can remove or emplace large-scale loads on the lithosphere, with consequences for the lateral flow of mantle material, and as a result, can produce tectonic features and modify topography [e.g., *Solomon and Head*, 1980; *Phillips et al.*, 2001; *Tanaka et al.*, 2001]. Three events that occurred in the northern lowlands during the Hesperian are very likely to have caused loading and unloading and thus to have had tectonic and topographic effects. The first event was the emplacement of approximately one kilometer thickness of Hesperian volcanic ridged plains in the Early Hesperian [*Head et al.*, 2002]. This level of load could have readily initiated subsidence and a peripheral bulge. Second, the outflow channel emplacement of a combined volume of sediment and water effluent of $\sim$600 m average thickness (on the basis of the average elevation of Contact 2 [*Head et al.*, 1999]) would have created a further load in the Late Hesperian, also potentially leading to subsidence and marginal bulges [see also *Tanaka et al.*, 2001]). Third, the geologically relatively rapid removal of a significant part of this outflow channel effluent load (Figure 4) could have led to rebound and a reversal of the topographic and tectonic trends, similar to the manner in which the emplacement and removal of Pleistocene ice sheets have operated in the recent geological past on Earth [e.g., *Peltier*, 1986]. Such effects might have included marginal highs associated with the Chryse outflow channel floors at the basin margins, tilting of the Utopia basin floor southward, variations in the present elevation of Contact 2 in different places along the margins [*Head et al.*, 1999; *Tanaka et al.*, 2001], and formation of polygonal terrains in the basin interior [e.g., *Hiesinger and Head*, 2000].

4.6. Implications for the Hesperian Hydrologic Cycle and Cryosphere

[90] *Parker et al.* [1989, 1993] and *Baker et al.* [1991] envisioned outflow channel effluents forming ocean-scale standing bodies of water that persisted for geologically significant periods of time during the Hesperian Period. We find no compelling evidence for the long-term presence of standing bodies of water. Instead, our analysis supports previous treatments [e.g., *Carr*, 1983; *Kargel et al.*, 1995; *Moore et al.*, 1995] that suggest that ponded outflow channel effluents would undergo rapid freezing and sublimation under both present conditions and conditions

envisioned for the Late Hesperian Period by most authors (see recent reviews by *Jakosky and Phillips* [2001] and *Baker* [2001]). Although frozen outflow channel effluent could escape sublimation up to the present if protected by a thick enough insulating layer [e.g., *Carr*, 1983; *Clifford*, 1993], we found no evidence to support the presence of such a layer, although local pockets of residual ice could persist on the floors of stealth craters underlying the Vastitas Borealis Formation (Figure 11).

[91] *Clifford and Parker* [2001] have suggested that during the Noachian a northern lowlands ocean was in direct communication with the groundwater table and that those conditions persisted until the Early Hesperian. Our analysis suggests that conditions during the Late Hesperian were such that cryospheric melting caused by emplacement of standing bodies of water was insufficient to melt through the cryosphere to develop communication (either draining of water into the groundwater table, or release of groundwater into the ocean), which is consistent with the scenario by *Clifford and Parker* [2001]. If Noachian-aged oceans existed, as envisioned by *Clifford and Parker* [2001], conditions at that time would be similar to those described for a Hesperian ocean as soon as a global cryosphere was formed. If any residual deposits remain in the northern lowlands from a proposed Noachian ocean (either ice, sediments, or a sublimation residue), they would lie below both the Vastitas Borealis Formation and the underlying sequence of Hesperian ridged plains.

[92] In summary, our analyses are consistent with conditions on the surface of Mars during the Late Hesperian being very similar to those of today (Figure 5), with temperatures well below freezing, atmospheric pressure well below values that would support liquid water for extended periods of time, and a cryosphere that is broadly similar to that of today, with thicknesses moderately less due to the higher geothermal gradient typical of the Late Hesperian [e.g., *Zuber et al.*, 2000; *Zuber*, 2001]. Even if temporary conditions permitting stable liquid water were caused by emplacement of the outflow channels [e.g., *Gulick et al.*, 1997], this would only decrease the residence time of an ocean, and would not substantially influence the structure of the cryosphere. Thus, by the Late Hesperian, the global hydrological cycle appears to be characterized by a thick global cryosphere much like that that exists today, one which effectively separates the groundwater reservoir from relatively minor surface migration caused by seasonal variations and obliquity cycles. If the outflow channels are correctly interpreted as representing the release of water from a confined subsurface aquifer by breaching of the cryosphere [e.g., *Carr*, 1979, 1996b], then this strongly implies that the groundwater table contained a significant amount of groundwater, and that it was in contact with the base of the cryosphere, at least regionally [e.g., *Clifford*, 1993; *Clifford and Parker*, 2001]. In this context, the advent of the outflow channels represents a major perturbation to the hydrologic cycle existing at that time, bringing subsurface water to the surface in vast quantities (of the order of 10^7 km^3). The vast majority of this water appears to have resided for a very short period of time in the northern lowlands, rapidly undergoing freezing and sublimation. Water sublimated during this process was deposited in other parts of the surface, and has formed part of the migrating surface water reservoir, including the polar deposits. Part of this water may have returned to the subsurface [e.g., *Clifford*, 1993; *Head and Pratt*, 2001]. Emplacement and redistribution could have influenced long-term obliquity variations on the scales of 10 Myr and longer [e.g., *Touma and Wisdom*, 1993; *Bills*, 1999].

4.7. Relation to Hypothesized Noachian Ocean

[93] Our treatment concerns the Late Hesperian-aged outflow channel effluent and its evolution. *Clifford and Parker* [2001] have described evidence for an earlier Noachian-aged ocean. They hypothesized that the existence of this primordial ocean was the inevitable consequence of the large inventory of H_2O and the hydraulic and thermal conditions thought to have existed throughout the first billion years of the history of Mars. They further hypothesized that the natural consequences of the evolution of post-Noachian climate and heat flow would be the freezing solid and subsequent assimilation of the resulting frozen ocean, a rise of the global groundwater table, and the catastrophic breakout of groundwater and reflooding of the northern lowlands during the Hesperian. To a first order, the evolution of this hypothesized Noachian northern lowlands ocean following its freezing would proceed along similar lines and timescales to that developed here for the Hesperian, with details depending on the exact climatic conditions existing in the Late Noachian. There is a possibility of preservation of frozen Noachian-aged ocean deposits, today potentially buried below the Upper Hesperian Vastitas Borealis Formation and the Lower Hesperian ridged plains.

4.8. Outstanding Problems

[94] Among the most important outstanding problems remain the ages of individual flooding events, the volumes of effluent involved, their sediment load, and their duration. Although the Upper Hesperian period is geologically short (about 400–600 million years in duration [*Hartmann and Neukum*, 2001; *Ivanov*, 2001]), available data suggest that the major outflow channel events in Chryse are separated by at least tens of millions of years [e.g., *Tanaka*, 1997], and this could readily exceed the lifetime of water effluent ponded in the northern lowlands under any of the conditions considered here, including standing liquid water [e.g., *Gulick et al.*, 1997] (Figures 4–5). Under the current range of estimates, the volume of individual channel-forming events could either fill the northern lowlands to the level of contact 2 of *Parker et al.* [1989, 1993] (approximately the edge of the Vastitas Borealis Formation) [e.g., *Baker et al.*, 1991] or represent a volume as small as 1/46th of this volume [e.g., *Ivanov and Head*, 2001].

[95] The thinness of the Vastitas Borealis Formation, the presence of Lower Hesperian ridged plains of apparent volcanic origin below it, the uniqueness of the Vastitas Borealis Formation roughness characteristics and its subunits on Mars, its Upper Hesperian temporal equivalence and lateral continuity with outflow channel deposits, all support its interpretation as the sedimentary deposit of the effluents of the outflow channels. Remaining unresolved is the detailed interpretation and understanding of individual occurrences and subunits of the Vastitas Borealis Formation, the origin of individual features composing the unit (e.g., the abundant small cones) and the ultimate fate of the water

that was involved in the emplacement of the outflow channel effluents.

[96] **Acknowledgments.** Reviews by Mike Carr and Steve Clifford were extremely helpful in the work on this paper. Thanks are extended to Kathryn Fishbaugh for valuable discussions and early investigations of aspects of this problem in a term paper, to Dmitry Stankevich, Natalia Bondarenko, Patrick Russell, and Stephen Pratt for valuable discussions, to Stephen Pratt for assistance in preparation of data and figures, and to Anne Côté for help in manuscript preparation. This work was supported by a grant to JWH from the Mars Data Analysis Program, which is gratefully acknowledged.

References

Aharonson, O., M. T. Zuber, G. A. Neumann, and J. W. Head, Mars: Northern hemisphere slopes and slope distributions, *Geophys. Res. Lett.*, *25*, 4413–4416, 1998.

Baker, V. R., Water and the Martian landscape, *Nature*, *412*, 228–236, 2001.

Baker, V. R., R. G. Strom, V. C. Gulick, J. S. Kargel, G. Komatsu, and V. S. Kale, Ancient oceans, ice sheets and the hydrological cycle on Mars, *Nature*, *352*, 589–594, 1991.

Bandfield, J. L., V. E. Hamilton, and P. R. Christensen, A global view of Martian surface compositions from MGS-TES, *Science*, *287*, 1626–1630, 2000.

Benn, D. I., and D. J. A. Evans, *Glaciers and Glaciation*, Oxford Univ. Press, New York, 1998.

Bills, B. G., Obliquity-oblateness feedback on Mars, *J. Geophys. Res.*, *104*, 30,773–30,797, 1999.

Bills, B. G., and T. S. James, Moments of inertia and rotational stability of Mars: Lithospheric support of subhydrostatic rotational flattening, *J. Geophys. Res.*, *104*, 9081–9096, 1999.

Binder, A. B., R. Arvidson, E. A. Guinness, K. L. Jones, E. C. Morris, T. A. Mutch, D. C. Pieri, and C. Sagan, The geology of the Viking Lander 1 site, *J. Geophys. Res.*, *82*, 4439–4451, 1977.

Brass, G. W., Stability of brines on Mars, *Icarus*, *42*, 20–28, 1980.

Carr, M. H., Retention of an atmosphere on early Mars, *J. Geophys. Res.*, *104*, 21,897–21,909, 1979.

Carr, M. H., Stability of streams and lakes on Mars, *Icarus*, *56*, 476–495, 1983.

Carr, M. H., D/H on Mars: Effects of floods, volcanism, impacts and polar processes, *Icarus*, *87*, 210–277, 1990.

Carr, M. H., *Water on Mars*, Oxford Univ. Press, New York, 1996a.

Carr, M. H., Channels and valleys on Mars: Cold climate features formed as a result of a thickening cryosphere, *Planet. Space Sci.*, *44*, 1411–1423, 1996b.

Carr, M. H., Retention of an atmosphere on early Mars, *J. Geophys. Res.*, *104*, 21,897–21,909, 1999.

Carr, M. H., and G. G. Schaber, Martian permafrost features, *J. Geophys. Res.*, *82*, 4039–4054, 1977.

Carr, M. H., S. U. Wu, R. Jordan, and F. J. Schafer, Volumes of channels, canyons and chaos in the circum-Chryse region of Mars (abstract), *Lunar Planet. Sci.*, *XVIII*, 155–156, 1987.

Chicarro, A. F., P. H. Schultz, and P. Masson, Global and regional ridge patterns on Mars, *Icarus*, *63*, 153–174, 1985.

Christensen, P. R., Regional dust deposits on Mars: Physical properties, age, and history, *J. Geophys. Res.*, *91*, 3533–3545, 1986a.

Christensen, P. R., The spatial distribution of rocks on Mars, *Icarus*, *68*, 217–238, 1986b.

Christensen, P. R., J. L. Bandfield, M. D. Smith, V. E. Hamilton, and R. N. Clark, Identification of a basaltic component on the Martian surface from Thermal Emission Spectrometer data, *J. Geophys. Res.*, *105*, 9609–9622, 2000.

Clifford, S. M., A model for hydrologic and climatic behavior of water on Mars, *J. Geophys. Res.*, *98*, 10,973–11,016, 1993.

Clifford, S. M., and T. J. Parker, Hydraulic and thermal arguments regarding the existence and fate of a primordial Martian ocean, *Lunar Planet. Sci.* [CD-ROM], *XXX*, abstract 1619, 1999.

Clifford, S. M., and T. J. Parker, The evolution of the Martian hydrosphere: Implications for the fate of a primordial ocean and the current state of the northern plains, *Icarus*, *154*, 40–79, 2001.

Cushman-Roisin, B., *Introduction to Geophysical Fluid Dynamics*, Prentice-Hall, Old Tappan, N. J., 1994.

Dial, A., Geologic map of the Mare Boreum region of Mars, *U.S. Geol. Surv. Misc. Invest. Ser., Map I-1640*, 1984.

Frey, H. V., and M. Jarosewich, Subkilometer Martian volcanoes: Properties and possible terrestrial analogs, *J. Geophys. Res.*, *87*, 9867–9879, 1982.

Garvin, J. B., J. J. Frawley, S. E. H. Sakimoto, and C. Schnetzler, Global geometric properties of Martian impact craters: An assessment from Mars Orbiter Laser Altimeter (MOLA) digital elevation models, *Lunar Planet. Sci.* [CD-ROM], *XXXI*, abstract 1619, 2000a.

Garvin, J. B., S. E. Sakimoto, J. J. Frawley, and C. Schnetzler, North polar region craterforms on Mars: Geometric characteristics from the Mars Orbiter Laser Altimeter, *Icarus*, *1444*, 329–352, 2000b.

Greeley, R., and J. E. Guest, Geologic map of the Eastern equatorial region of Mars, *U.S. Geol. Surv. Misc. Invest. Ser., Map I-1802-B*, 1987.

Greeley, R., M. Kraft, R. Sullivan, G. Wilson, N. Bridges, K. Herkenhoff, R. O. Kuzmin, M. Malin, and W. Ward, Aeolian features and processes at the Mars Pathfinder landing site, *J. Geophys. Res.*, *104*, 8573–8584, 1999.

Gulick, V. C., D. Tyler, C. P. McKay, and R. M. Haberle, Episodic ocean-induced CO_2 greenhouse on Mars: Implications for fluvial valley formation, *Icarus*, *130*, 68–86, 1997.

Hartmann, W. K., and G. Neukum, Cratering chronology and evolution of Mars, *Space Sci. Rev.*, *95*, 167–196, 2001.

Head, J. W., and M. A. Kreslavsky, Medusae Fossae Formation as volatile-rich airborne material deposited during outflow events and/or periods of high obliquity, *34th Vernadsky-Brown Microsymposium* [CD-ROM], abstract MS025, Brown Univ., Providence, R. I., 2001a.

Head, J. W., and M. A. Kreslavsky, Medusae Fossae Formation as volatile-rich sediments deposited during high obliquity: An hypothesis and tests, paper presented at Conference on the Geophysical Detection of Subsurface Water on Mars, abstract 7053, Lunar and Planet. Inst., Houston, Tex., 2001b.

Head, J. W., and R. T. Pappalardo, Brine mobilization during lithospheric heating on Europa: Implications for formation of chaos terrain, lenticulae texture, and color variations, *J. Geophys. Res.*, *104*, 27,143–27,155, 1999.

Head, J. W., and S. Pratt, Extensive Hesperian-aged south polar ice sheet on Mars: Evidence for massive melting and retreat, and lateral flow and ponding of meltwater, *J. Geophys. Res.*, *106*(E6), 12,275–12,300, 2001.

Head, J. W., H. Hiesinger, M. A. Ivanov, M. A. Kreslavsky, S. Pratt, and B. Thomson, Possible ancient oceans on Mars: Evidence from Mars Orbiter Laser Altimeter data, *Science*, *286*, 2134–2137, 1999.

Head, J. W., S. Bigler, and S. Pratt, Small knobs and cones in Isidis Planitia and the Northern Lowlands: Description and stratigraphic relationships, *34th Vernadsky-Brown Microsymposium* [CD-ROM], abstract MS026, Brown Univ., Providence, R. I., 2001.

Head, J. W., M. A. Kreslavsky, and S. Pratt, Northern lowlands of Mars: Evidence for widespread volcanic flooding and tectonic deformation in the Hesperian Period, *J. Geophys. Res.*, *107*(E1), 5003, doi:10.1029/2000JE001445, 2002.

Hiesinger, H., and J. W. Head, Characteristics and origin of polygonal terrain in southern Utopia Planitia, Mars: Results from Mars Orbiter Laser Altimeter and Mars Orbiter Camera data, *J. Geophys. Res.*, *105*(E5), 11,999–12,022, 2000.

Hobbs, P. V., *Ice Physics*, Oxford Univ. Press, New York, 1974.

Hoffman, N., White Mars: A new model for Mars' surface and atmosphere based in CO_2, *Icarus*, *146*, 326–342, 2000.

Hoffman, N., K. L. Tanaka, J. S. Kargel, and W. B. Banerdt, Emplacement of a debris ocean on Mars by regional-scale collapse and flow at the crustal dichotomy, *Lunar Planet. Sci.* [CD-ROM], *XXXII*, abstract 1584, 2001.

Ivanov, A. B., and D. O. Muhleman, The role of sublimation for the formation of the northern ice cap: Results from the Mars Orbiter Laser Altimeter, *Icarus*, *144*, 436–448, 2000.

Ivanov, B. A., Mars/Moon cratering rate ratio estimates, *Space Sci. Rev.*, *96*, 87–104, 2001.

Ivanov, M. A., and J. W. Head, Chryse Planitia, Mars: Topographic configuration, outflow channel continuity and sequence, and tests for hypothesized ancient bodies of water using Mars Orbiter Laser Altimeter (MOLA) data, *J. Geophys. Res.*, *106*(E2), 3275–3295, 2001.

Jakosky, B. M., and R. M. Haberle, The seasonal behavior of water on Mars, in *Mars*, edited by H. H. Kieffer et al., pp. 969–1016, Univ. of Ariz. Press, Tucson, 1992.

Jakosky, B. M., and R. J. Phillips, Mars' volatile and climate history, *Nature*, *412*, 237–244, 2001.

Kargel, J. S., V. R. Baker, J. E. Beget, J. F. Lockwood, T. L. Pewe, J. S. Shaw, and R. G. Strom, Evidence of continental glaciation in the Martian northern plains, *J. Geophys. Res.*, *100*, 5351–5368, 1995.

Komatsu, G., J. S. Kargel, V. R. Baker, R. G. Strom, G. G. Ori, C. Mosangini, and K. L. Tanaka, A chaotic terrain formation hypothesis: Explosive outgas and outlow by dissociation of clathrate on Mars, *Lunar Planet. Sci.* [CD-ROM], *XXXI*, abstract 1434, 2000.

Kreslavsky, M. A., and J. W. Head, Kilometer-scale slopes on Mars and their correlation with geologic units: Initial results from Mars Orbiter Laser Altimeter (MOLA) data, *J. Geophys. Res.*, *104*, 21,911–21,924, 1999.

Kreslavsky, M. A., and J. W. Head, Kilometer-scale roughness of Mars' surface: Results from MOLA data analysis, *J. Geophys. Res.*, *105*, 26,695–26,712, 2000.

Lanagan, P. D., A. S. McEwen, L. P. Keszthelyi, and T. Thordarson, Rootless cones on Mars indicating the presence of shallow equatorial ground ice in recent times, *Geophys. Res. Lett.*, *28*, 2365–2367, 2001.

Laskar, J., and P. Robutel, The chaotic obliquity of the planets, *Nature*, *361*, 608–612, 1993.

Leshin, L. A., Insights into Martian water reservoirs from analyses of Martian meteorite QUE94201, *Geophys. Res. Lett.*, *27*, 2017–2020, 2000.

Lindström, E. F., F. Sturkell, R. Törnberg, and J. Ormö, The marine impact crater at Lockne, central Sweden, *Geol. Fören. Stockholm Förh.*, *118*, 193–206, 1996.

McSween, H. Y., Basalt or andesite? A critical evaluation of constraints on the composition of the ancient Martian crust, *Lunar Planet. Sci.* [CD-ROM], *XXXIII*, abstract 1062, 2002.

Mellon, M. T., and B. M. Jakosky, Geographic variations in the thermal and diffusive stability of ground ice on Mars, *J. Geophys. Res.*, *98*, 3345–3364, 1993.

Mellon, M. T., and B. M. Jakosky, The distribution and behavior of Martian ground ice during past and present epochs, *J. Geophys. Res.*, *100*, 11,781–11,799, 1995.

Melosh, H. J., and A. M. Vickery, Impact erosion of the primordial Martian atmosphere, *Nature*, *338*, 487–489, 1989.

Milton, D. J., Carbon dioxide hydrate and floods on Mars, *Science*, *183*, 654–656, 1974.

Moore, J. M., G. D. Clow, W. L. Davis, V. C. Gulick, D. R. Janke, C. P. McKay, C. R. Stoker, and A. P. Zent, The circum-Chryse region as a possible example of a hydrologic cycle on Mars: Geologic observations and theoretical evaluation, *J. Geophys. Res.*, *100*, 5433–5447, 1995.

Mustard, J. F., C. D. Cooper, and M. K. Rifkin, Evidence for recent climate change on Mars from the identification of youthful near-surface ground ice, *Nature*, *412*, 411–414, 2001.

Mutch, T. A., R. Arvidson, A. B. Binder, E. A. Guinness, and E. C. Morris, The geology of the Viking Lander 2 site, *J. Geophys. Res.*, *82*, 4452–4467, 1977.

Noble, S. K., and C. M. Pieters, Type 2 terrain: Compositional constraints on the Martian lowlands, *Lunar Planet. Sci.* [CD-ROM], *XXXII*, abstract 1230, 2001.

Owen, T., The composition and early history of the atmosphere of Mars, in *Mars*, edited by H. H. Kieffer et al., pp. 818–834, Univ. of Ariz. Press, Tucson, 1992.

Parker, T. J., R. S. Saunders, and D. M. Schneeberger, Transitional morphology in West Deuteronilus Mensae, Mars: Implications for modification of the Lowland/Upland boundary, *Icarus*, *82*, 111–145, 1989.

Parker, T. J., D. S. Gorsline, R. S. Saunders, D. C. Pieri, and D. M. Schneeberger, Coastal geomorphology of the Martian northern plains, *J. Geophys. Res.*, *98*, 11,061–11,078, 1993.

Peltier, W. R., Deglaciation induced vertical motion of the North American continent and transient lower mantle rheology, *J. Geophys. Res.*, *91*, 9099–9123, 1986.

Pepin, R. O., Evolution of the Martian atmosphere, *Icarus*, *111*, 289–304, 1994.

Phillips, R. J., et al., Ancient geodynamics and global-scale hydrology on Mars, *Science*, *291*, 2587–2591, 2001.

Pollack, J. B., et al., Properties and effects of dust particles suspended in the Martian atmosphere, *J. Geophys. Res.*, *84*, 2929–2945, 1979.

Russell, P. S., and J. W. Head, The Elysium/Utopia flows: Characteristics from topography and a model of emplacement, *Lunar Planet. Sci.* [CD-ROM], *XXXII*, abstract 1040, 2001.

Russell, P. S., and J. W. Head, The Martian hydrosphere/cryosphere system: Implications of the absence of hydrologic activity at Lyot Crater, *Lunar Planet. Sci.* [CD-ROM], *XXXIII*, abstract 1688, 2002.

Schultz, P. H., and A. B. Lutz, Polar wandering of Mars, *Icarus*, *73*, 91–141, 1988.

Scott, D. H., and K. L. Tanaka, Geologic map of the Western Equatorial region of Mars, *U.S. Geol. Surv. Misc. Invest. Ser., Map I-1802-A*, 1986.

Smith, D. E., et al., Topography of the northern hemisphere of Mars from the Mars Orbiter Laser Altimeter, *Science*, *279*, 1686–1691, 1998.

Smith, D. E., et al., The global topography of Mars and implications for surface evolution, *Science*, *284*, 1495–1503, 1999.

Solomon, S. C., and J. W. Head, Lunar mascon basins: Lava filling, tectonics and evolution of the lithosphere, *Rev. Geophys.*, *18*, 107–141, 1980.

Squyres, S. W., S. M. Clifford, R. O. Kuzmin, J. R. Zimbelman, and F. M. Costard, Ice in Martian regolith, in *Mars*, edited by H. H. Kieffer et al., Univ. of Ariz. Press, Tucson, 1992.

Tanaka, K. L., Sedimentary history and mass flow structure of Chryse and Acidalia Planitiae, Mars, *J. Geophys. Res.*, *102*, 4131–4149, 1997.

Tanaka, K. L., and D. H. Scott, Geologic map of the Polar Regions of Mars, *U.S. Geol. Surv. Misc. Invest. Ser., Map I-1802-C*, 1987.

Tanaka, K. L., M. G. Chapman, and D. H. Scott, Geologic map of the Elysium Region of Mars, *U.S. Geol. Surv. Misc. Invest. Ser., Map I-2147*, 1992.

Tanaka, K. L., W. B. Banerdt, J. S. Kargel, and N. Hofman, Huge, CO_2-charged debris-flow deposit and tectonic sagging in the northern plains of Mars, *Geology*, *29*, 427–430, 2001.

Tanaka, K. L., J. A. Skinner, T. M. Hare, T. Joyal, and A. Wenker, Resurfacing of the northern plains of Mars by shallow subsurface, volatile driven activity, *Lunar Planet. Sci.* [CD-ROM], *XXXIII*, abstract 1406, 2002.

Thatje, S., D. Gerdes, and E. Rachor, A seafloor crater in the German Bight and its effects on the benthos, *Helgoland Mar. Res.*, *53*, 36–44, 1999.

Thomas, P., S. Squyres, K. Herkenhoff, A. Howard, and B. Murray, Polar deposits of Mars, in *Mars*, edited by H. H. Kieffer et al., pp. 767–795, Univ. of Ariz. Press, Tucson, 1992.

Thomson, B., and J. W. Head, Utopia Basin, Mars: Characterization of topography and morphology and assessment of the origin and evolution of basin internal structure, *J. Geophys. Res.*, *106*, 23,209–23,230, 2001.

Toon, O. B., J. B. Pollack, W. Ward, J. A. Burns, and K. Bilski, The astronomical theory of climatic change on Mars, *Icarus*, *44*, 552–607, 1980.

Touma, J., and J. Wisdom, The chaotic obliquity of Mars, *Science*, *259*, 1294–1297, 1993.

Ward, W. R., Long-term orbital and spin dynamics of Mars, in *Mars*, edited by H. H. Kieffer et al., pp. 298–320, Univ. of Ariz. Press, Tucson, 1992.

Wilson, L., and J. W. Head, Mars: Review and analysis of volcanic eruption theory and relationships to observed landforms, *Rev. Geophys.*, *32*, 221–263, 1994.

Wilson, L., and J. W. Head III, Heat transfer and melting in subglacial basaltic volcanic eruptions: Implications for volcanic deposit morphology and meltwater volumes, in *Volcano-Ice Interaction on Earth and Mars*, *Geol. Soc. Spec. Publ.*, in press, 2002.

Wyatt, M. B., J. L. Bandfield, H. Y. McSween, P. R. Christensen, and J. Moersch, TES observations of Chryse and Acidalia Planitiae: Multiple working hypotheses for distributions of surface compositions, *Lunar Planet. Sci.* [CD-ROM], *XXXIII*, abstract 1554, 2002.

Zuber, M. T., The crust and mantle of Mars, *Nature*, *412*, 220–227, 2001.

Zuber, M. T., et al., Internal structure and early thermal evolution of Mars from Mars Global Surveyor topography and gravity, *Science*, *287*, 1788–1793, 2000.

J. W. Head and M. A. Kreslavsky, Department of Geological Sciences, Brown University, Box 1846, Providence, RI 02912-1846, USA. (james_head_III@brown.edu)